AGU PUBLICATIONS

JGR

Journal of Geophysical Research: Atmospheres

RESEARCH ARTICLE

10.1002/2016JD026309

Key Points:
- Aerosol direct radiative effects on $PM_{2.5}$ concentrations in the NCP were simulated
- The boundary layer heights averaged over the NCP reduced by 19.4% and 10.8%, respectively, due to scattering aerosols and BC
- $PM_{2.5}$ concentrations averaged over the NCP increased by 16.8% and 1.0%, respectively, due to scattering aerosols and BC

Supporting Information:
- Supporting Information S1

Correspondence to:
H. Liao,
hongliao@nuist.edu.cn

Citation:
Qiu, Y., H. Liao, R. Zhang, and J. Hu (2017), Simulated impacts of direct radiative effects of scattering and absorbing aerosols on surface layer aerosol concentrations in China during a heavily polluted event in February 2014, *J. Geophys. Res. Atmos.*, *122*, 5955–5975, doi:10.1002/2016JD026309.

Received 1 DEC 2016
Accepted 10 MAY 2017
Accepted article online 11 MAY 2017
Published online 5 JUN 2017

Simulated impacts of direct radiative effects of scattering and absorbing aerosols on surface layer aerosol concentrations in China during a heavily polluted event in February 2014

Yulu Qiu[1,2], Hong Liao[3,4], Renjian Zhang[5], and Jianlin Hu[3]

[1]State Key Laboratory of Atmospheric Boundary Layer Physics and Atmospheric Chemistry (LAPC), Institute of Atmospheric Physics, Chinese Academy of Sciences, Beijing, China, [2]University of Chinese Academy of Sciences, Beijing, China, [3]School of Environmental Science and Engineering, Nanjing University of Information Science and Technology, Nanjing, China, [4]Joint International Research Laboratory of Climate and Environment Change, Nanjing University of Information Science and Technology, Nanjing, China, [5]Key Laboratory of Regional Climate-Environment Research for Temperate East Asia, Institute of Atmospheric Physics, Chinese Academy of Sciences, Beijing, China

Abstract We quantified aerosol direct radiative effects on surface layer concentrations of aerosols during a heavily polluted event in the North China Plain (NCP, 35.4°N–41.2°N, 113.3°E–119.3°E) during 21–27 February 2014, using the chemistry version of the Weather Research and Forecasting (WRF-Chem) Model. Comparisons of model results with observations showed that the WRF-Chem model reproduced the spatial and temporal variations of meteorological variables reasonably well, but overestimated average $PM_{2.5}$ concentration by 21.7% over the NCP during 21–27 February. The simulated direct radiative effects of total, absorbing, and scattering aerosols reduced the planetary boundary layer (PBL) heights by 111.4 m, 35.7 m, and 70.7 m, respectively, averaged over NCP and 21–27 February. The direct radiative effects of total aerosols induced increases in aerosol concentrations by 11.5% for SO_4^{2-}, 29.5% for NO_3^-, 29.6% for NH_4^+, 28.7% for organic carbon (OC), 26.7% for black carbon (BC), and 20.4% for $PM_{2.5}$, respectively, averaged over the NCP during 21–27 February 2014. The increase in $PM_{2.5}$ concentration averaged over the NCP and the haze event was 29.6 μg m^{-3} (16.8%) due to radiative effect of scattering aerosols, as a result of the decreases in PBL height and changes in secondary aerosol production rates. The corresponding increase in $PM_{2.5}$ concentration owing to absorbing aerosols was 2.1 μg m^{-3} (1.0%), resulting from the offsetting impacts of changes in PBL height, wind near the surface, and chemical processes.

1. Introduction

High concentrations of aerosols, also referred to as particulate matter, lead to adverse health impacts [*Yadav et al.*, 2003; *Tie et al.*, 2009], reductions in visibility [*Schichtel et al.*, 2001; *Chen et al.*, 2003; *Chan and Yao*, 2008], and radiative forcing on regional and global scale [*Giorgi et al.*, 2002; *Jung et al.*, 2009; *Liao et al.*, 2015; *K. Li et al.*, 2015]. Due to the rapid economic and industrial development over the past three decades, severe haze events have been frequently observed in the North China Plain (NCP) during autumn and winter [*X. J. Zhao et al.*, 2013; *Y. S. Wang et al.*, 2014; *Sun et al.*, 2014; *Zhang et al.*, 2014; *Yang et al.*, 2015; *Wang et al.*, 2016; *Yang et al.*, 2016]. For example, *Y. S. Wang et al.* [2014] reported that the observed maximum hourly $PM_{2.5}$ concentration in Beijing reached 680 μg m^{-3} during an extremely severe haze event on 12 January 2013. These high surface layer concentrations of $PM_{2.5}$ during autumn and winter in China are caused by the high anthropogenic emissions and the stable synoptic conditions. Meteorological conditions, such as weak surface winds, low planetary boundary layer (PBL) height, and high relative humidity, play important roles in the formation of heavily polluted episodes [*Wang et al.*, 2006; *Niu et al.*, 2010; *X. J. Zhao et al.*, 2013; *Quan et al.*, 2014].

Previous observational studies have reported the chemical characteristics of aerosols during haze periods over the NCP region [*X. J. Zhao et al.*, 2013; *Sun et al.*, 2014; *Zhang et al.*, 2016]. *X. J. Zhao et al.* [2013] showed that total concentrations of sulfate (SO_4^{2-}), nitrate (NO_3^-), and ammonium (NH_4^+) were 127.0 and 113.5 μg m^{-3} in Tianjin and Beijing, respectively, averaged over 14–23 January 2010, accounting for 44.8 and 33.7% of total $PM_{2.5}$ concentrations. *Sun et al.* [2014] reported that the observed percentages of inorganic aerosol concentrations ($SO_4^{2-} + NO_3^- + NH_4^+$ + chloride (Cl^-)) in PM_1 were elevated from 31% during clean periods

(with averaged PM_1 concentrations of 13.8 μg m^{-3}) to 40–54% during haze episodes (with averaged PM_1 concentrations of 144–300 m^{-3}) in Beijing in January 2013. *Zhang et al.* [2016] observed the aerosol composition in Beijing from 4 August to 3 September 2012 and showed that the averaged concentrations of SO_4^{2-}, NO_3^-, and NH_4^+ were 4.5, 4.0, and 4.2 times higher than those during nonhaze days, respectively. The haze days were defined as days with observed $PM_{2.5}$ concentrations higher than 75 μg m^{-3} and observed atmospheric visibility less than 10 km at a RH lower than 90%. Furthermore, the percentage increases in inorganic aerosols were greater than the percentage increase of total $PM_{2.5}$ concentrations during haze days relative to nonhaze days. This suggests that secondary inorganic aerosols play important roles in the formation of haze.

Aerosols can scatter or absorb solar radiation (i.e., aerosol direct radiative effect), leading to changes in the Earth's radiative balance and in meteorological fields. Previous studies have reported large changes in shortwave radiative fluxes during heavily polluted events [*Che et al.*, 2014; *H. Wang et al.*, 2014]. Based on Cimel Sun photometer measurements at seven sites over the North China Plain, *Che et al.* [2014] reported that the maximum daily mean direct aerosol radiative effect at the surface within the solar zenith angles of 50–80° during the intensely polluted period of 10–16 January 2013, exceeded −50, −180, and −200 W m^{-2} at rural, suburban, and urban sites, respectively. Large reductions in radiative fluxes at the surface during severe pollution events have decreased surface temperatures and reduced PBL height [*Ding et al.*, 2013; *Liao and Liao*, 2014; *H. Wang et al.*, 2014]. Using comprehensive measurements during an intense air pollution event in Nanjing, China, and the Weather Research and Forecasting (WRF) Model, *Ding et al.* [2013] found that the total impact of mixed agricultural burning plumes, together with fossil fuel combustion pollution during 9–11 June 2012, resulted in a maximum decrease in temperature by almost 10 K and a decrease in PBL height. *H. Wang et al.* [2014] examined the interactions between aerosols and PBL during a haze episode in July 2008, over the NCP region using the new-generation Global/Regional Assimilation and PrEdiction System (GRAPES), developed by the China Meteorological Administration and the Chinese Unified Atmospheric Chemistry Environment (GRAPES_CUACE). They found that the percentage changes in PBL heights between simulations with and without aerosol direct radiative effects were −33%.

Aerosol radiative effects can influence surface layer aerosol concentrations [*Forkel et al.*, 2012], especially during pollution events [*J. Wang et al.*, 2014; *Gao et al.*, 2015; *Ding et al.*, 2016; *Gao et al.*, 2016a], through feedbacks onto meteorological fields. *J. Wang et al.* [2014] analyzed the response of $PM_{2.5}$ species to aerosol radiative effects during a haze event in the NCP region in January 2013 using the WRF-CMAQ model. They found that when considering the aerosol direct radiative effect, the surface layer concentrations of NO_3^-, SO_4^{2-}, NH_4^+, BC, and OC increased by 15.2%, 20.4%, 18.5%, 30.3%, and 30.2%, respectively. Primary aerosols (BC and OC) showed significant increases greater than the secondary aerosols (NO_3^-, SO_4^{2-} and NH_4^+) due to the complex formation mechanisms of secondary aerosols. *Gao et al.* [2015] investigated the impact of aerosol radiative effects on surface concentrations of $PM_{2.5}$ using the WRF-Chem model in the NCP region in January 2013. They found that aerosol radiative effects increased surface layer $PM_{2.5}$ by 10–50 μg m^{-3} (2–30%) when averaged over 10–15 January over the NCP region due to the decreased PBL height. With high concentrations of BC observed in the NCP region, the radiative impacts of absorbing aerosols were simulated to increase surface layer $PM_{2.5}$ concentrations as a result of the depressed development of PBL induced by BC heating in the upper boundary layer [*Ding et al.*, 2016; *Gao et al.*, 2016a]. *Gao et al.* [2016a] reported that $PM_{2.5}$ concentration increased by about 14.4 μg m^{-3} through BC absorption in Shijiazhuang (38.0°N, 114.5°E). This accounted for approximately 65.7% of $PM_{2.5}$ changes due to the feedback of all aerosols.

Scattering and absorbing aerosols have different radiative impacts [*Chang and Liao*, 2009; *C. Zhao et al.*, 2013; *Gao et al.*, 2014]. As mentioned above, although there are several studies demonstrating the impacts of absorbing aerosols on $PM_{2.5}$ concentrations, few studies have separately examined the impacts of both scattering and absorbing aerosols on the chemical components of $PM_{2.5}$. Different aerosols have different formation processes (for example, increases in temperature enhance the chemical production of SO_4^{2-} in the atmosphere [*Aw and Kleeman*, 2003; *Dawson et al.*, 2007; *Kleeman*, 2008] and decrease NO_3^- formation [*Liao et al.*, 2006; *Racherla and Adams*, 2006; *Bellouin et al.*, 2011]). It is therefore important to understand how scattering and absorbing aerosols affect individual aerosol species during severe haze days.

To examine the impacts of aerosol direct radiative effects on air quality, we used the online-coupled regional chemistry-climate model WRF-Chem. The goal of this study was to examine systematically the aerosol direct radiative feedbacks on $PM_{2.5}$ components in the NCP region during a severe haze event in 21–27 February 2014. We paid special attention to (1) the spatial and temporal variations of aerosol direct radiative feedbacks on meteorological variables and major aerosol species during the severe haze event and (2) the separate roles of the radiative effects of scattering and absorbing aerosols.

This paper is organized as follows. The WRF-Chem model, experimental configuration, and observational data sets used in the study are described briefly in section 2. Section 3 compares simulated meteorological and chemical variables with observations. The impacts of aerosol-meteorological feedbacks of total, scattering, and absorbing aerosols in meteorological fields, $PM_{2.5}$ species, and other atmospheric species are examined in section 4. We discuss the uncertainties of this study in section 5.

2. Model Configuration and Observation Data

2.1. WRF-Chem Model

This study used version 3.6.1 of WRF-Chem [*Grell et al*., 2005; *Fast et al*., 2006; *Chapman et al*., 2009] to simulate meteorological fields and concentrations of gas phase species and aerosols simultaneously. The WRF-Chem model was configured with three nested domains, with grid resolutions of 90, 30, and 10 km (Figure 1), respectively. The inner domain covered the NCP region with 33 vertical layers up to 50 hPa. We used the gas phase chemistry scheme of the CBM-Z mechanism [*Zaveri and Peters*, 1999], with photolysis rates calculated using the Fast-J scheme [*Wild et al*., 2000]. For the aerosol module, the Model for Simulating Aerosol Interactions and Chemistry (MOSAIC) [*Zaveri et al*., 2008] with eight sizes of bins (0.039–0.078, 0.078–0.156, 0.156–0.3125, 0.3125–0.625, 0.625–1.25, 1.25–2.5, 2.5–5.0, and 5.0–10 μm) was used. The aerosol species treated in MOSAIC included NO_3^-, SO_4^{2-}, NH_4^+, BC, OC, sodium (Na^+), Cl^-, and other inorganics (OIN). In the current MOSAIC module, secondary organic aerosol (SOA) was not included. Aerosols were internally mixed in each bin, and externally mixed among eight bins. The sectional treatment of aerosols also had impacts on aerosol optical properties. In the optical module, all components except BC were assumed to be uniformly distributed in a shell that surrounded a core consisting only of BC [*Barnard et al*., 2010]. Dry deposition of trace gases and aerosol particles were based on the methods of *Wesely* [1989] and *Binkowski and Shankar* [1995], respectively. In-cloud aerosols and gases were removed by using the first-order loss rate of cloud water from the microphysics scheme. Wet deposition of gases and aerosols below cloud followed the method of *Easter et al.* [2004], in which aerosol impaction/interception scavenging rates were size dependent.

The major physical parameterizations in this study included the Rapid Radiative Transfer Model for GCMs (RRTMG) shortwave and longwave radiation schemes [*Zhao et al*., 2011], the modified Purdue Lin microphysics module [*Lin et al*., 1983], the Noah Land Surface Model scheme, and the Yonsei University (YSU) planetary boundary layer scheme [*Hong et al*., 2006]. Our simulation of SO_4^{2-} followed that in *X. Huang et al.* [2014], who implemented the SO_2 aqueous oxidation catalyzed by iron (Fe) and manganese (Mn) to improve the representation of SO_4^{2-} aerosol over eastern China in the WRF-Chem model [*X. Huang et al*., 2014].

2.2. Emission Inventories

Anthropogenic emissions were taken from the Hemispheric Transport of Air Pollution (HTAP) version 2 global inventory, which consisted of monthly emissions of nitrogen oxides (NO_x), carbon monoxide (CO), non-methane volatile organic compounds (NMVOC), sulfur dioxide (SO_2), ammonia (NH_3), primary PM_{10}, primary $PM_{2.5}$, BC, and OC for year 2010 with a horizontal resolution of 0.1° [*M. Li et al*., 2015]. In February, the anthropogenic emissions of NO_x, CO, NMVOC, SO_2, NH_3, primary PM_{10}, primary $PM_{2.5}$, BC, and OC were, respectively, 1.95, 16.13, 1.81, 2.05, 0.51, 1.32, 1.03, 0.17, and 0.38 Tg species over eastern China (20.0°N–45.0°N, 98.0°E–125.0°E). We assumed that the emissions in year 2010 were the same as those in year 2014. Anthropogenic emissions were assumed to be emitted at the surface. Biogenic emissions were calculated from the Model of Emissions of Gases and Aerosols from Nature (MEGAN) [*Guenther et al*., 2006]. Biomass burning emissions were taken from the Fire INventory from NCAR (FINN) datasets [*Wiedinmyer et al*., 2011]. Emissions of sea salt and dust were calculated online following *Gong et al.* [1997; 2003] and *Zhao et al.* [2010], respectively.

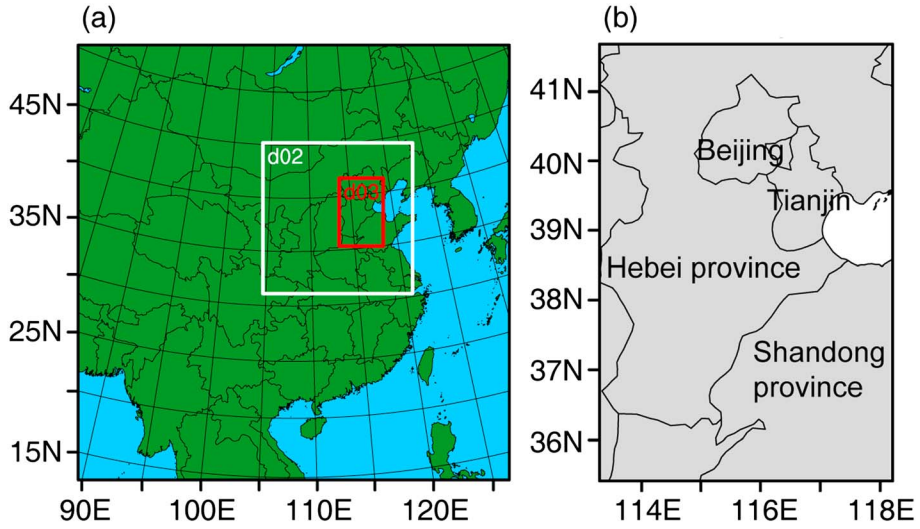

Figure 1. Model domains. (a) The area within the red square indicates the NCP region (35.4°N–41.2°N, 113.3°E–119.3°E) at 10 km resolution. The area within the white square is simulated at 30 km resolution, and the rest of the East Asian domain is simulated at 90 km resolution. (b) Locations of Beijing, Tianjin, Hebei, and Shandong provinces.

2.3. Numerical Experiments

To examine the direct radiative effects of scattering and absorbing aerosols on the simulated surface layer concentrations of aerosols, we performed the following simulations for the time period of 21–27 February 2014.

1. CTRL: The control simulation of meteorological parameters and chemistry/aerosols with coupled aerosol direct and indirect radiative effects.
2. noALL: The same as the CTRL simulation, except that the direct radiative effect of all aerosols was turned off over the three nested model domains.
3. noABS: The same as the CTRL simulation, except that the direct effect of absorbing aerosol (BC) was turned off. Although dust is usually treated as the light-absorbing aerosol in previous studies, it is still difficult to separate the optical contribution of dust from the total OIN aerosol. This is because the OIN aerosol consists of the unspeciated primary aerosol and dust in both the MOSAIC aerosol module and the optical module of the WRF-Chem model. Therefore, only BC was treated as the absorbing aerosol in our study.
4. noSCAT: The same as the CTRL simulation except that the direct effect of scattering aerosols (NO_3^-, SO_4^{2-}, NH_4^+, OC, Na^+, Cl^-, OIN, and aerosol water) was turned off.
5. CTRL_0.5BC: The same as the CTRL simulation, except that BC emissions were reduced by 50% over the three nested model domains.
6. noABS_0.5BC: The same as the noABS simulation, except that BC emissions were reduced by 50% over the three nested model domains.

The aerosol direct radiative effect was turned off by removing the mass of aerosol species from the calculation of aerosol optical properties, which did not influence the simulation of the aerosol indirect effect in the simulations above. The difference in the model results between CTRL and noALL simulations (CTRL–noALL) represented the direct radiative effect of all aerosols on meteorology and concentrations of chemical species. The radiative effects of scattering and absorbing aerosols were quantified by the differences between CTRL and noSCAT (CTRL–noSCAT), and CTRL and noABS (CTRL–noABS), respectively. The difference between the CTRL_0.5BC and noABS_0.5BC cases (CTRL_0.5BC–noABS_0.5BC) was used to determine the uncertainties associated with the radiative impact of BC. The initial and boundary meteorological conditions were provided by the National Centers for Environmental Prediction (NCEP) 1° × 1° reanalysis data. The initial and boundary conditions of chemical species were derived from the results of the Model for Ozone and Related chemical Tracers, version 4 (MOZART-4) [*Emmons et al.*, 2010]. For each simulation, the model was first spun up for 64 h and then integrated and analyzed over 0000 local time (LT) 21 February to 0000 LT 28 February 2014. We have used LT in this paper unless stated otherwise.

2.4. Observation Data

Meteorological and chemical observation data sets were used to evaluate the model performance in the NCP region. For meteorological variables, the surface meteorological data were obtained from NOAA's National Climatic Data Center (https://gis.ncdc.noaa.gov/maps/ncei/cdo/hourly), which consisted of temperature at 2 m (T2), relative humidity at 2 m (RH2), wind speed at 10 m (WS10), and wind direction at 10 m (WD10). We used 18 measurement stations (see Table S1 in the supporting information) in the NCP region in this study. Beijing radiosonde data, provided by the University of Wyoming, Department of Atmospheric Science (http://weather.uwyo.edu/upperair/sounding.html), were also used to evaluate the simulated temperature profiles.

Surface concentrations of $PM_{2.5}$, NO_2, SO_2, and O_3 during 21–27 February 2014 were obtained from the China National Environmental Monitoring Center (CNEMC). Concentrations of speciated aerosols (SO_4^{2-}, NO_3^-, NH_4^+, BC, and OC) from 24 to 27 February 2014, were collected at the Tower Division of the Institute of Atmospheric Physics, Chinese Academy of Sciences, in Beijing (40.0°N, 116.3°E). This observation site is approximately 8 m above ground level and is a typical urban site surrounded by residential areas. Besides, concentrations of $PM_{2.5}$ components in Jinan (36.7°N, 117.1°E) during 21–27 February were also obtained from *Chen et al.* [2016]. Aerosol optical depth (AOD) at 550 nm from the AERONET data set [*Holben et al.*, 1998] was used to evaluate the simulated aerosol optical properties.

3. Simulated Haze Event and Model Evaluation

3.1. Concentrations of $PM_{2.5}$, SO_2, NO_2, and O_3

Figure 2a shows the observed and simulated spatial distributions of $PM_{2.5}$, SO_2, NO_2, and O_3 from the CTRL simulation over the NCP and averaged over 21–27 February. Observations are shown for 19 cities from the CNEMC. Observed $PM_{2.5}$ concentrations showed highest values of 300–400 $\mu g\ m^{-3}$ in the western Hebei Province. Observed concentrations of aerosol precursors of SO_2 and NO_2 had high values in Tianjin, western and northern Hebei, and northern Shandong provinces, with SO_2 concentrations of 100–180 $\mu g\ m^{-3}$ and NO_2 concentrations of 80–140 $\mu g\ m^{-3}$ averaged over 21–27 February (Figure 2a). Observed O_3 concentrations were low over most of the NCP region with values of 20–60 $\mu g\ m^{-3}$ averaged between 21 and 27 February (Figure 2a). The model performed well in simulating the spatial distributions of the mean concentrations of $PM_{2.5}$ and other gas species (SO_2, NO_2, and O_3) averaged between 21 and 27 February in the 19 cities in the NCP (Figure 2a).

Figure 2b shows the observed and simulated time series of hourly concentrations of $PM_{2.5}$, SO_2, NO_2, and O_3 averaged over the 19 cities during 21–27 February. Both observed and simulated concentrations peaked on 25 February for all four species. The model reproduced the temporal variations of $PM_{2.5}$, SO_2, NO_2, and O_3 during 21–27 February with correlation coefficients (*Rs*) between simulated and observed hourly concentrations of 0.85, 0.78, 0.71, and 0.67, respectively. Compared with observations, the simulated concentrations of $PM_{2.5}$, SO_2, NO_2, and O_3 had mean biases (MBs) and normalized mean biases (NMBs; in brackets) of 44.0 $\mu g\ m^{-3}$ (21.7%), 1.5 $\mu g\ m^{-3}$ (1.3%), −3.6 $\mu g\ m^{-3}$ (−4.7%), and 16.7 $\mu g\ m^{-3}$ (66.1%), respectively.

Because of the lack of measurements of speciated aerosols for the whole NCP, Figure 3 compares the simulated surface layer mass concentrations of SO_4^{2-}, NO_3^-, BC, OC, and NH_4^+ from the CTRL simulation versus observations in Beijing and Jinan during the haze event. The observed concentrations of SO_4^{2-}, NO_3^-, NH_4^+, BC, and OC in Beijing were available only for 24–27 February 2014 (section 2.4). Therefore, the observed and simulated concentrations in Beijing were averaged between 24 and 27 February for comparison. In Beijing (Jinan), the model underestimated the concentrations of NH_4^+, OC, and SO_4^{2-} by 6.3% (27.9%), 23.5% (24.4%), and 66% (68.7%), respectively, and overestimated the concentrations of BC and NO_3^- by 92.8% (91.9%) and 60.7% (47.4%), respectively. For OC, the underestimation may have resulted from the lack of representation of SOA in the MOSAIC aerosol module. For SO_4^{2-} the underestimation occurred with an overestimation of SO_2 concentrations by about 161% in Beijing, although the model captured SO_2 well in the NCP (Figure 2). Considering that the simulated total concentration of SO_4^{2-}, NO_3^-, and NH_4^+ agreed closely with observations with a MB (NMB) of 2.1–15.8 $\mu g\ m^{-3}$ (1.5–14.1%) and that these three aerosol species had approximately the same optical properties [*Barnard et al.*, 2010], the model biases in the concentrations of speciated aerosols should not influence the simulation of the direct effect of these three types of aerosols.

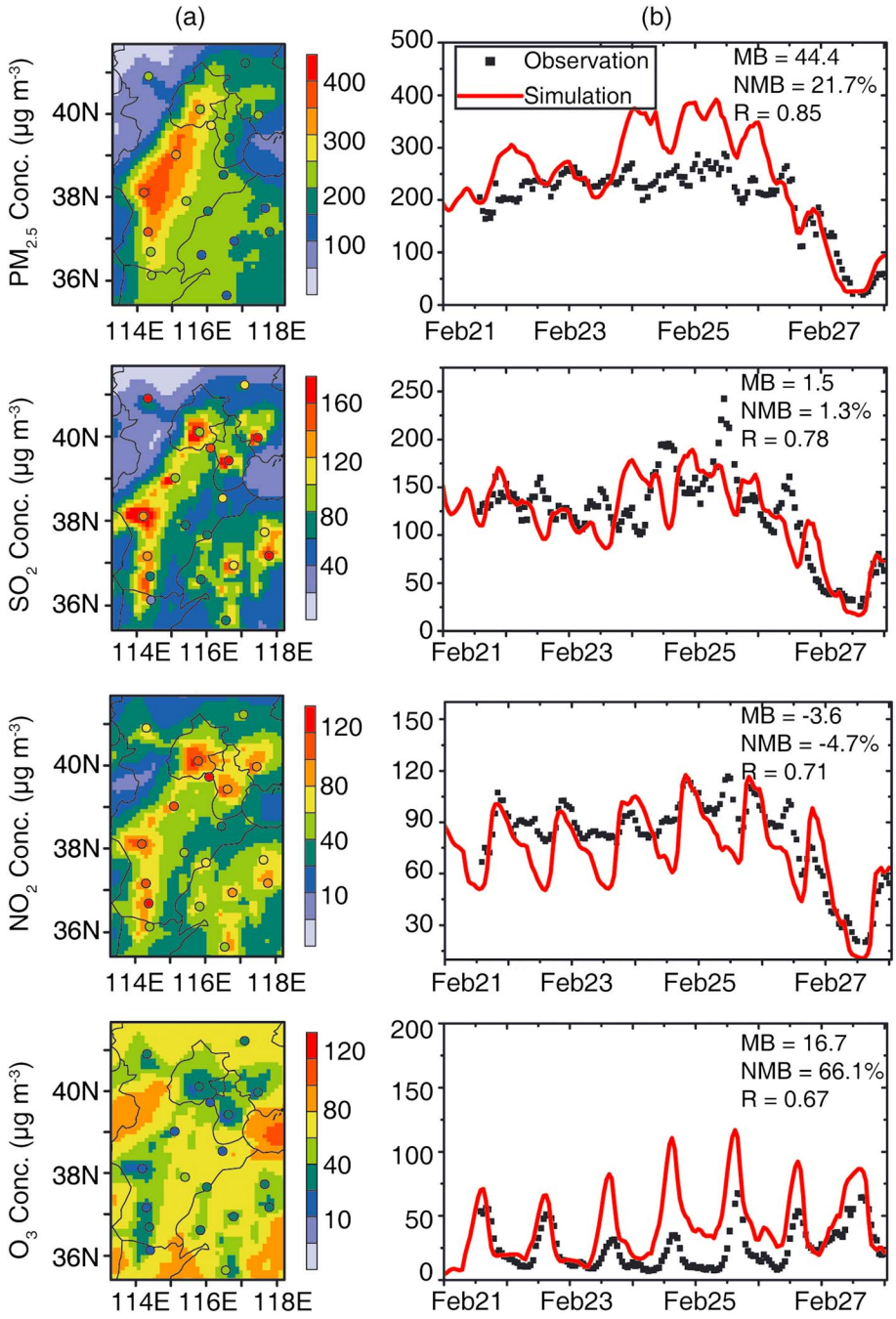

Figure 2. (a) Simulated spatial distributions of concentrations (μg m^{-3}) of $PM_{2.5}$, SO_2, NO_2, and O_3 in the NCP, averaged over 21–27 February 2014. Overlaid are the observed concentrations (circles) at the 19 stations averaged over these same dates. (b) Time series of observed (black dots) and simulated (red lines) hourly concentrations (μg m^{-3}) of $PM_{2.5}$, SO_2, NO_2, and O_3 averaged over the 19 stations in the NCP. Also shown in Figure 2b are the mean bias (MB), normalized mean bias (NMB), and correlation coefficient (R) for each panel. $MB = \left[\sum_{i=1}^{N}(P_i - O_i)\right]/N$, $NMB = \left[\sum_{i=1}^{N}(P_i - O_i)\right]/\left(\sum_{i=1}^{N}O_i\right)\cdot 100\%$, where P_i and O_i are the predicted and observed concentrations of a chemical species (i.e., $PM_{2.5}$, SO_2, NO_2, or O_3), respectively. The parameter i refers to the ith hour and N is the total number of hours.

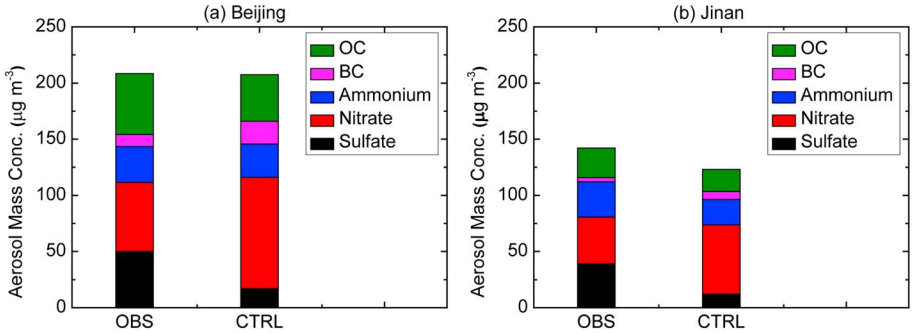

Figure 3. Comparison of observed and simulated surface layer mass concentrations (μg m^{-3}) of SO_4^{2-}, NO_3^-, NH_4^+, BC, and OC in (a) Beijing averaged over 24–27 February and in (b) Jinan averaged over 21–27 February.

The high bias in the simulated BC may have led to overestimation of the absorbing effect of BC, which will be addressed in section 5 when we discuss the uncertainties of our model simulation.

3.2. Meteorological Parameters

Figure 4 shows the simulated geopotential height at 500 hPa and wind at 850 hPa from the CTRL simulation at 2 A.M. for 21–27 February 2014. From 21 to 26 February, eastern China was covered by weak southwesterly winds in the boundary layer. The southwesterly winds transported aerosols and their precursors from the southern NCP to the mountain-plain area of northern NCP [*X. J. Zhao et al.*, 2013; *Y. S. Wang et al.*, 2014; *Gao et al.*, 2016a].

During this period, aerosols and other atmospheric pollutants accumulated in the PBL. On 27 February, a low-pressure system with strong northerly winds and severe cold air dominated the NCP region, which blew the pollutants away from the area. Figure 5 shows the simulated vertical profiles of hourly temperature, relative humidity, and wind speed averaged over the NCP during 21–27 February 2014. A strong temperature inversion occurred over the NCP region at nighttime on 22 February and during 24–26 February, which inhibited vertical mixing (Figure 5a). The corresponding $PM_{2.5}$ concentrations at the surface were highest on these dates (Figure 2). During 22–26 February, RH exceeded 50% in the lower troposphere ($<$ 700 hPa), which favored the formation of severe haze. The haze event was also accompanied by low wind speed ($<$ 3 m s^{-1}) in the PBL. These meteorological conditions contributed to the formation of the severe haze event, as reported in the previous studies of *Y. S. Wang et al.* [2014] and *Quan et al.* [2014]. On 27 February, temperature and RH decreased, and wind speed increased, which were all unfavorable for pollutant accumulation in the boundary layer.

Figure 6 shows the 3-hourly time series of simulated and observed T2, RH2, WS10, and WD10 averaged over the 18 stations in the NCP for 21–27 February 2014. The locations of the 18 stations that were available from NOAA's National Climatic Data Center are shown in Table S1 in the supporting information. Table 1 summarizes the statistics of the model performance in simulating meteorological parameters at the 18 stations during the study period. The model reproduced the temporal variation of T2 well (Figure 6) with a *R* value of 0.96 (Table 1), but underestimated T2 with a MB of −2.3°C. For RH2, the model results and observations showed high values of 70–90% at nighttime during 21–26 February, with a small MB of 3.1% and a *R* of 0.82. The model results and observations exhibited relatively low wind speed during 21–26 February and high wind speed on 27 February; however, the model overestimated wind speed with a NMB of 58.6%. Similar high biases in wind speed have been reported in previous studies using the WRF-Chem model over China and other countries [*Zhang et al.*, 2010; *Jiang et al.*, 2012; *Situ et al.*, 2013; *Liao et al.*, 2015; *Zhang et al.*, 2014; *Gao et al.*, 2015], which may have been caused by the default surface land cover type in WRF-Chem [*Yu et al.*, 2012; *Wang et al.*, 2012]. For WD10, the model-simulated southerly wind for 21–26 February and northerly wind on 27 February, which was consistent with the observations. In general, the model can predict the surface meteorological variables fairly well in the NCP.

Figure 7 compares the simulated vertical profiles of temperature with atmospheric radiosonde observations in Beijing (40.0°N, 116.3°E) at 8 A.M. and 8 P.M. for 22, 24, and 26 February 2014. The radiosonde observations were only available at these two local hours. A temperature inversion occurred on 24 and 26 February below

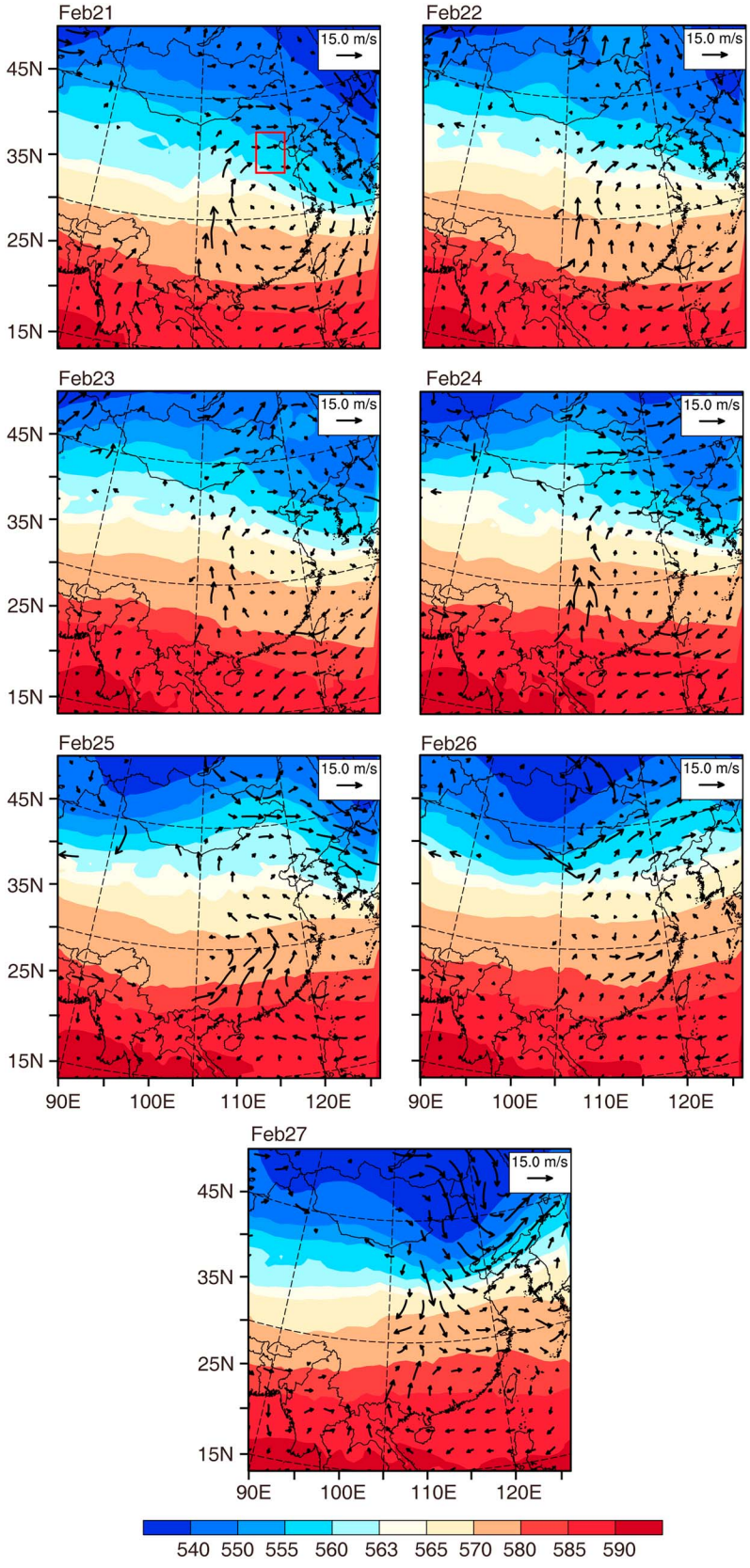

Figure 4. Simulated geopotential height (units: 10 gpm) at 500 hPa and wind field (m s^{-1}) at 850 hPa at 2 A.M. on each day during 21–27 February 2014. Red square in the first panel denotes the NCP region.

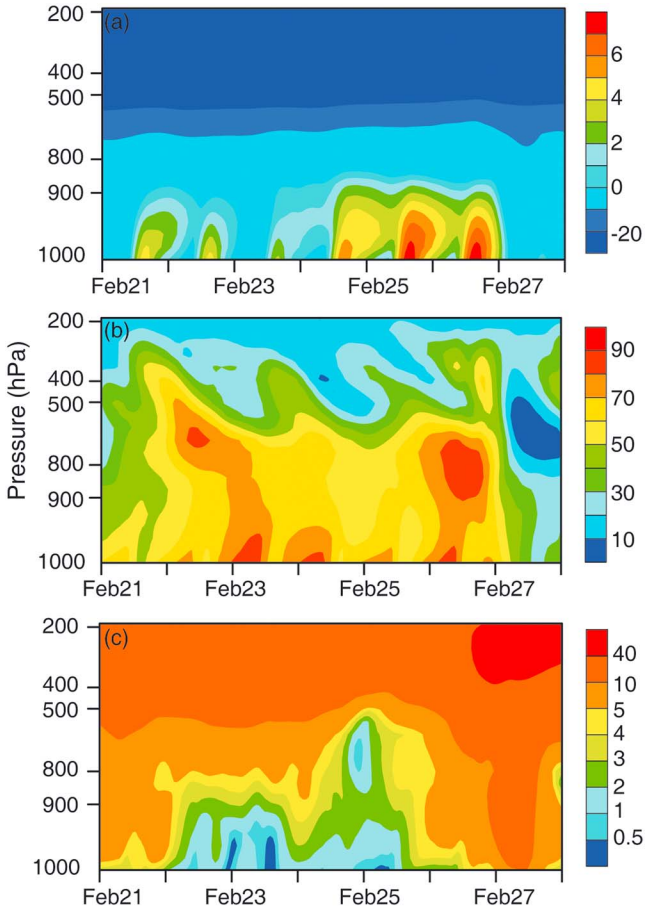

Figure 5. Simulated hourly vertical profiles of (a) temperature (°C), (b) relative humidity (%), and (c) wind speed (m s^{-1}). All parameters are averaged over the NCP during 21–27 February 2014.

1500 m, which was captured by the model. However, the model underestimated the inversion layer height on 24 February, which may have led to the overestimation of the $PM_{2.5}$ concentrations shown in Figure 2.

3.3. Aerosol Optical Depth

Previous studies found that MODIS retrievals tended to overestimate AOD in the NCP during polluted events compared with AERONET AOD [*Gao et al.*, 2015; *Li et al.*, 2016; *Miao et al.*, 2016]. Therefore, we are mainly focused on the comparisons between simulated AOD values and AERONET observations in this work. During 21–27 February, AERONET AOD observations were available at Xinglong station (40.39°N, 117.58°E) for days of 24, 26, and 27 February. The AERONET AOD values at 550 nm at Xinglong on 24, 26, and 27 February were 1.68, 1.20, and 0.08, respectively. The corresponding AOD values in the CTRL simulation were 0.60, 1.40, and 0.20, respectively. Simulated AOD value at Xinglong averaged over these three days had a low bias of −25.7% in comparison with AERONET AOD. Similar underestimation of AOD in comparison with AERONET observation in the NCP during haze events was also reported in previous studies [*Gao et al.*, 2015; *Miao et al.*, 2016], which might be caused by the representation of aerosol mixing state and refractive index in the WRF-Chem model [*Barnard et al.*, 2010; *Curci et al.*, 2015].

4. Feedback Effects of Aerosols

4.1. Simulated Direct Radiative Impacts of Aerosols on Meteorological Variables

In this section, we investigated the interactions between aerosols and meteorology by examining the differences between the CTRL simulation and the sensitivity simulations (noALL, noABS, and noSCAT). Figure 8 displays the spatial distributions of changes in the downward shortwave flux at the surface, T2, RH2, PBL height, and wind at 10 m in the NCP induced by the direct radiative effects of total (Figure 8a), absorbing (Figure 8b) and scattering (Figure 8c) aerosols. All changes were averaged over 21–27 February 2014. The shortwave radiation fluxes at the surface over the NCP were reduced by 54.6 W m^{-2}, 18.0 W m^{-2}, and 36.1 W m^{-2} by total, absorbing, and scattering aerosols, respectively, when averaged over NCP and between 21 and 27 February 2014. The corresponding reductions in T2 were 1.7°C, 0.2°C, and 1.6°C, respectively. In the simulation, RH2 increased by 4.1%, 0.9%, and 3.3% by total, absorbing, and scattering aerosols, respectively, when averaged over the NCP between 21 and 27 February. This resulted from the decrease in saturation vapor pressure due to the decreases in T2. A slight warming of T2 of 0.1–0.4°C occurred in the simulation in the northwestern NCP by absorbing aerosol, leading to reductions in RH2 by 2–4% in that region. The PBL heights averaged over the NCP between 21 and 27 February decreased by 111.4 m, 35.7 m, and 70.7 m, respectively, in the presence of all, absorbing, and scattering aerosols.

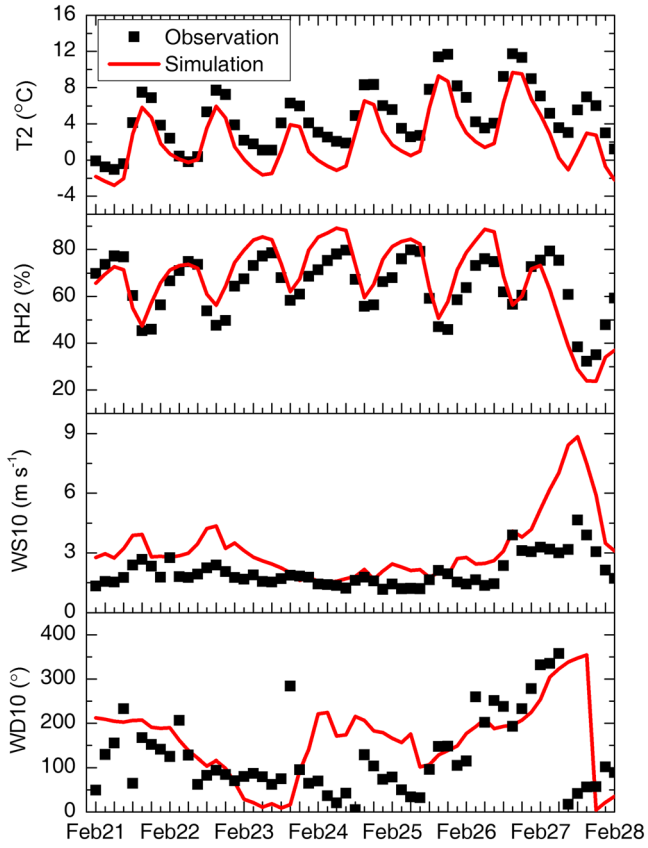

Figure 6. The 3-hourly time series of observed (black dots) and simulated (red lines) temperature at 2 m (T2; °C), relative humidity at 2 m (RH2; %), wind speed at 10 m (WS10; m s^{-1}), and wind direction at 10 m (WD10; deg). All parameters are averaged over the 18 stations (see Table S1) in the NCP for 21–27 February 2014.

We also show in Figure 8 the differences in wind at 10 m in the NCP due to the direct radiative effects of aerosols. Relative to the CTRL simulation, absorbing aerosols induced strong anomalous northeasterlies in the eastern NCP, while scattering aerosols had a small impact on winds in this region. The changes in wind can be explained by the changes in atmospheric temperature and pressure. For example, in the presence of absorbing aerosol, T2 increased by about 0.2–0.6°C in eastern China, leading to decreases in surface pressure of 40–90 Pa (Figure S1). Therefore, BC absorption induced anomalous cyclonic circulation near the surface and the corresponding northeasterlies in the eastern NCP. These changes in horizontal wind induced by the heating effect of BC were also reported in *Gao et al.* [2016a].

Figure 9 shows the time series of hourly direct radiative impacts of total, absorbing, and scattering aerosols on meteorological variables averaged over NCP during 21–27 February. Maximum changes for T2, RH2, and PBL height occurred in the daytime (9 A.M.–6 P.M.) when the maximum reductions in shortwave flux occurred at the surface. There were greater changes in T2, RH2, and PBL height during 21–26 February, which were

Table 1. Mean Bias (MB) and Normalized Mean Bias (NMB) of the Simulated Temperature at 2 m (T2; °C), Relative Humidity at 2 m (RH2; %), and Wind Speed at 10 m (WS10; m s^{-1}) Against the Observations at the 18 Stations in the NCP[a]

	SIM	OBS	R	MB	NMB
T2 (°C)	2.3	4.7	0.96	−2.3	N.A.
RH2 (%)	67.5	64.4	0.82	3.1	4.8%
WS10 (m s^{-1})	3.2	2.0	0.84	1.2	58.6%

[a]The simulated results (SIM) and observations (OBS) are the averages for the 18 stations between 21 and 27 February 2014. The correlation coefficients (*R*) are calculated between simulations and observations using the 3-hourly time series of the meteorological parameters averaged over the 18 stations for 21–27 February 2014. N.A., not applicable.

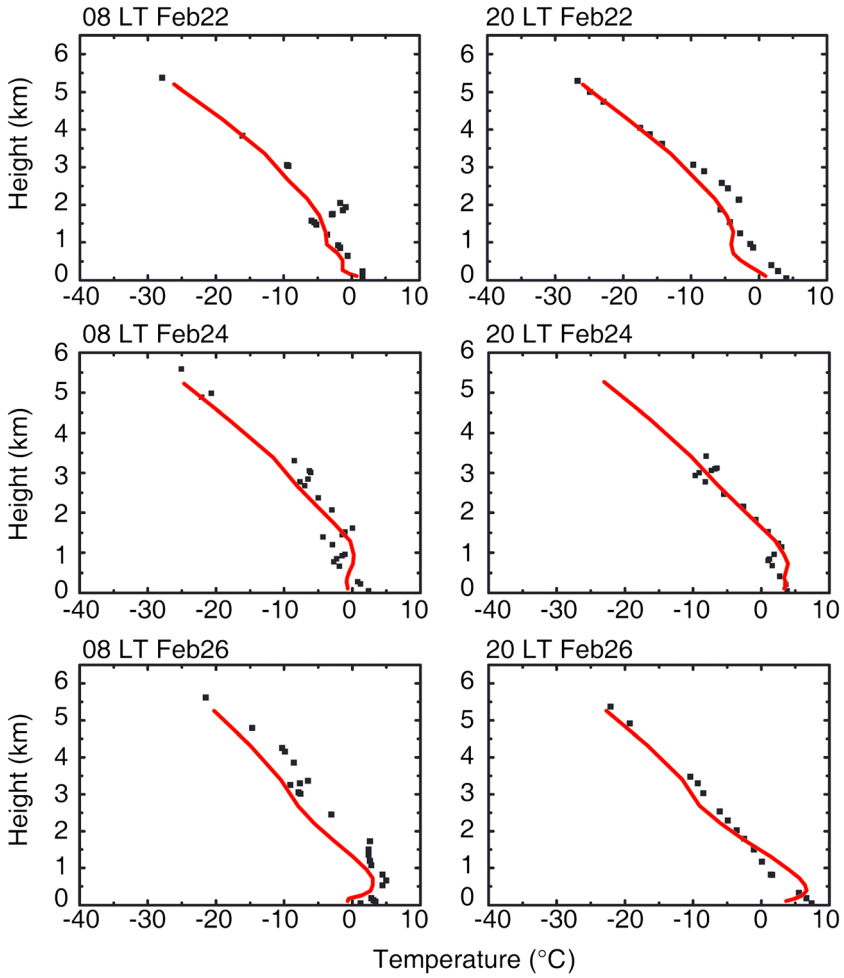

Figure 7. Observed (black dots) and simulated (red lines) temperature profiles in Beijing (39.9°N, 116.3°E) at 8 A.M. and 8 P.M. on 22, 24, and 26 February 2014.

consistent with the high $PM_{2.5}$ concentrations of 160–290 μg m^{-3} averaged over the NCP. Overall, the impacts of scattering aerosols on meteorology were greater than those of the absorbing aerosols due to the larger contribution of scattering aerosols to $PM_{2.5}$ mass concentration. However, as shown in Figure 9, the influence of absorbing aerosols on meteorology is important, even though BC accounts for less than 10% of the total aerosol mass concentration.

In this study, the aerosol direct radiative effects led to reductions in the shortwave flux at the surface in Beijing by 120–180 W m^{-2} in the daytime, averaged over 21–27 February 2014. Our results are, to some extent, consistent with those of *Che et al.* [2014], who showed that the daytime shortwave fluxes at the surface in Beijing decreased by 50–200 W m^{-2} with observed $PM_{2.5}$ concentrations of 100–500 μg m^{-3} during 10–15 January 2013. During 21–27 February 2014, our simulated daytime decreases in T2 in Beijing were about 2–3.4°C, which were higher than the reductions reported by *Gao et al.* [2015]. *Gao et al.* [2015] simulated the haze event in Beijing during 10–15 January 2013 and found that the mean decreases in daytime shortwave flux at the surface were 60–100 W m^{-2} and the reductions in T2 were 0.8–1.6°C. The differences between our results and *Gao et al.* [2015] can be explained by our higher simulated $PM_{2.5}$ concentrations (100–500 μg m^{-3}) in Beijing during 21–27 February 2014, relative to the simulated $PM_{2.5}$ concentrations of 50–250 μg m^{-3} in Beijing during 10–15 January 2013, in *Gao et al.* [2015].

In addition to the impacts on surface meteorology, aerosol direct radiative effects can induce large changes in atmospheric stability. Figure 10 shows the changes in the vertical profiles of the equivalent potential temperature (EPT) averaged over the NCP and 21–27 February 2014. Scattering aerosols cooled the surface (EPT

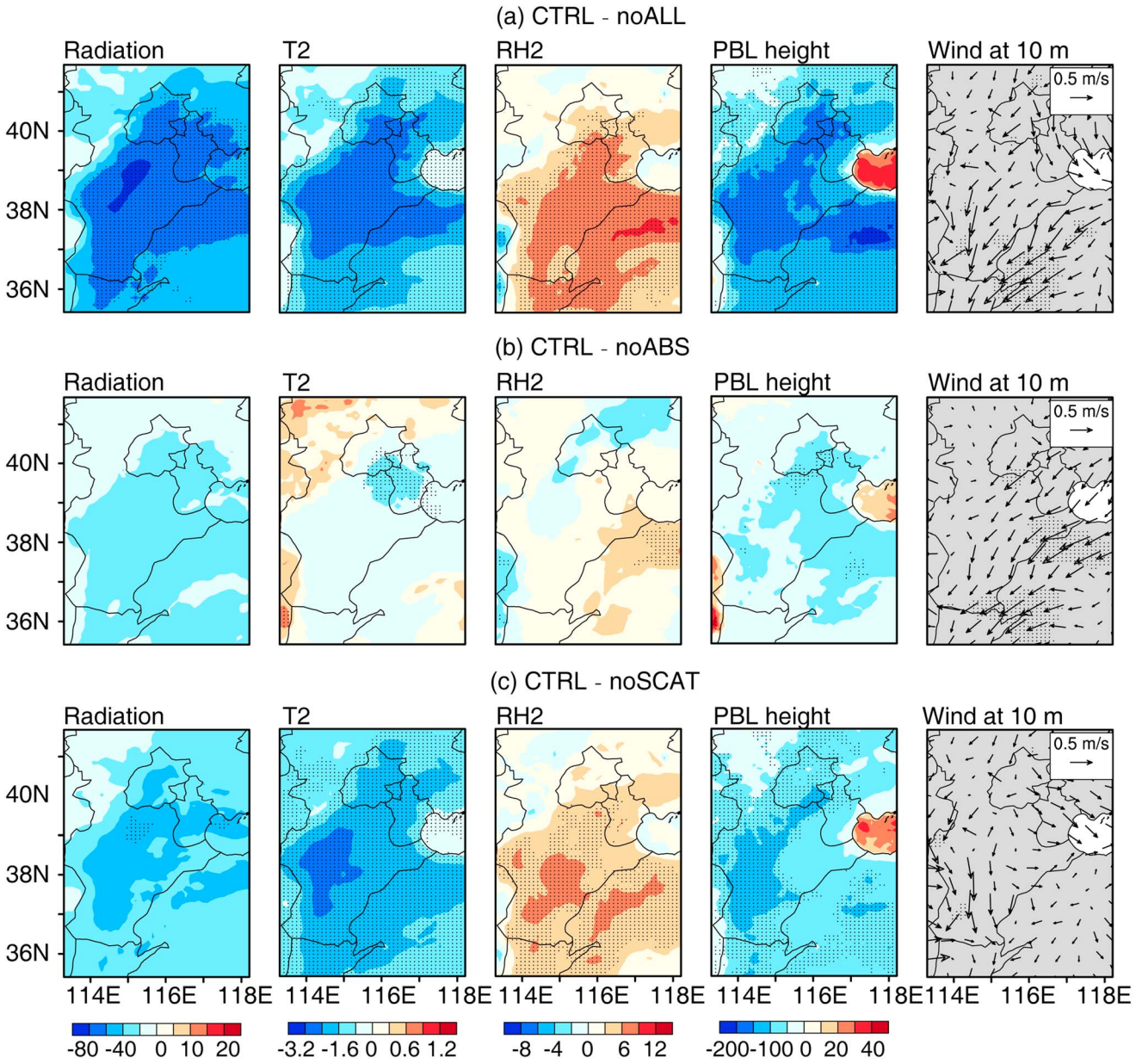

Figure 8. Changes in radiative flux (W m^{-2}), temperature at 2 m (T2; °C), relative humidity (RH2; %), planetary boundary layer (PBL) height (m), and wind at 10 m caused by the direct radiative effects of (a) total, (b) absorbing, and (c) scattering aerosols in the NCP averaged during 21–27 February 2014. The dotted areas are statistically significant at the 95% level, as determined by a two-sample Student's *t* test.

reduction of about 2.1°C), while BC warmed the upper boundary layer by approximately 0.6°C at 900 hPa, both of which led to a more stable atmosphere. The difference in EPT between 850 hPa and the surface (EPT at 850 hPa minus that at the surface) was larger for scattering aerosols than for absorbing aerosols, indicating that the atmosphere was more stable with scattering aerosols alone than with just absorbing aerosols.

4.2. Simulated Direct Radiative Impacts of Aerosols on $PM_{2.5}$ and Its Components

By altering the meteorological variables, aerosols exert feedbacks onto the concentrations of aerosols and other chemical species. Figure 11 shows the impact on surface layer aerosol components and $PM_{2.5}$ by direct radiative effects of total, absorbing, and scattering aerosols averaged over 21–27 February 2014, for NCP. With the direct radiative effects of all aerosols, the concentration increased 1.2 μg m^{-3} (11.5%) for SO_4^{2-},

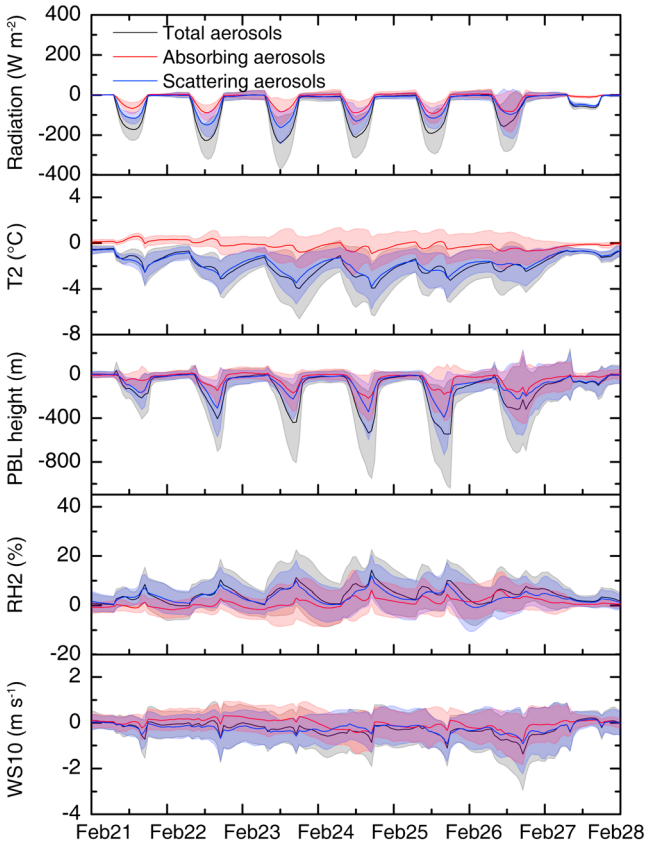

Figure 9. Hourly time series of changes in downward shortwave flux at the surface (W m^{-2}), temperature at 2 m (T2; °C), relative humidity at 2 m (RH2; %), planetary boundary layer (PBL) height (m), and wind speed at 10 m (WS10; m s^{-1}) caused by the direct radiative effects of total, absorbing, and scattering aerosols. The hourly values were averaged in the NCP during 21–27 February 2014. Shaded areas denote the standard deviation.

13.4 μg m^{-3} (29.5%) for NO_3^-, 2.6 μg m^{-3} (29.6%) for NH_4^+, 5.2 μg m^{-3} (28.7%) for OC, 4.6 μg m^{-3} (26.7%) for BC, and 34.9 μg m^{-3} (20.4%) for $PM_{2.5}$, as the values were averaged over the whole NCP region and 21–27 February 2014. Compared with the direct radiative effects of total aerosols, those induced by scattering aerosols led to similar spatial distributions, but smaller magnitudes of change in the aerosol

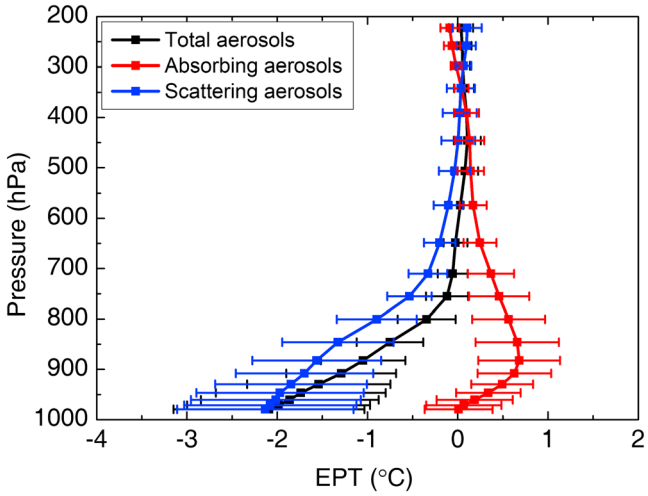

Figure 10. Changes in vertical profiles of the equivalent potential temperature (EPT) due to the direct radiative effects of total (black), absorbing (red), and scattering aerosols (blue) averaged over the NCP and during 21–27 February 2014. The whiskers denote the standard deviation.

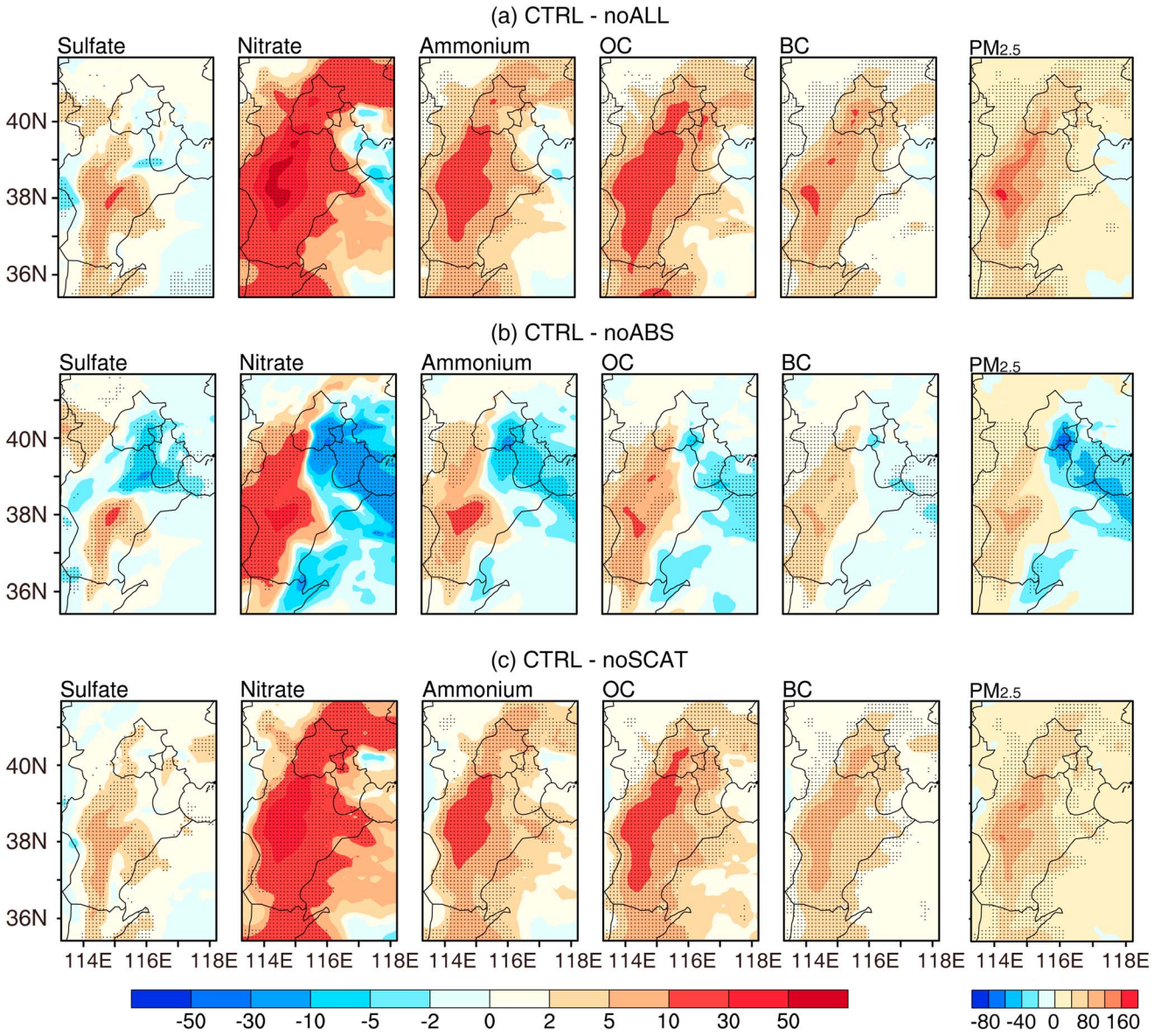

Figure 11. Spatial distributions of changes in the surface layer concentrations ($\mu g\ m^{-3}$) of $PM_{2.5}$ and its components (SO_4^{2-}, NO_3^-, NH_4^+, OC, and BC) due to the direct radiative effects of (a) total, (b) absorbing, and (c) scattering aerosols averaged during 21–27 February 2014. The dotted areas are statistically significant at the 95% level, as determined by a two-sample Student's *t* test.

concentrations (except for SO_4^{2-}). The mean increases were 1.4 $\mu g\ m^{-3}$ (13.5%) for SO_4^{2-}, 11.2 $\mu g\ m^{-3}$ (23.4%) for NO_3^-, 2.1 $\mu g\ m^{-3}$ (22.7%) for NH_4^+, 4.2 $\mu g\ m^{-3}$ (22.3%) for OC, 3.9 $\mu g\ m^{-3}$ (22.1%) for BC, and 29.6 $\mu g\ m^{-3}$ (16.8%) for $PM_{2.5}$, respectively. With the direct radiative effect of BC, concentrations of SO_4^{2-}, NO_3^-, NH_4^+, OC, BC, and $PM_{2.5}$ increased over the western and southern Hebei Province. The maximum increases were 5–20 $\mu g\ m^{-3}$ for SO_4^{2-}, 15–40 $\mu g\ m^{-3}$ for NO_3^-, 5–25 $\mu g\ m^{-3}$ for NH_4^+, 5–20 $\mu g\ m^{-3}$ for OC, 2–7 $\mu g\ m^{-3}$ for BC, and 20–120 $\mu g\ m^{-3}$ for $PM_{2.5}$, respectively. However, the radiative effect of BC led to reductions in $PM_{2.5}$ and its components in eastern NCP, with the largest reductions of 2–15 $\mu g\ m^{-3}$ for SO_4^{2-}, 5–30 $\mu g\ m^{-3}$ for NO_3^-, 2–15 $\mu g\ m^{-3}$ for NH_4^+, 2–10 $\mu g\ m^{-3}$ for OC, 0.5–5 $\mu g\ m^{-3}$ for BC, and 20–80 $\mu g\ m^{-3}$ for $PM_{2.5}$, respectively. Therefore, the mean changes in aerosol concentrations due to the direct radiative effects of absorbing aerosols, averaged over the NCP region and 21–27 February 2014, were −0.2 $\mu g\ m^{-3}$ (−1.9%) for SO_4^{2-}, 0.8 $\mu g\ m^{-3}$ (1.3%) for NO_3^-, 0.4 $\mu g\ m^{-3}$ (4.1%) for NH_4^+, 0.7 $\mu g\ m^{-3}$ (3.2%) for OC, 0.3 $\mu g\ m^{-3}$ (3.1%) for BC,

and 2.1 μg m^{-3} (1.0%) for $PM_{2.5}$, respectively. These were much lower than the increases induced by the direct radiative effects of scattering aerosols.

Averaged over 21–27 February the simulated changes in $PM_{2.5}$ concentration due to the direct radiative effect of total aerosols were 15–80 μg m^{-3} in the Beijing area, which were higher than the changes in $PM_{2.5}$ of 5–40 μg m^{-3} in Beijing in *Gao et al.* [2015]. *J. Wang et al.* [2014] reported that SO_4^{2-}, NO_3^-, NH_4^+, OC, and BC in Beijing averaged over 12–24 January 2013, increased by 15.2%, 20.4%, 18.5%, 30.2%, and 30.3%, respectively, compared with the concentrations simulated without aerosol direct effect. Our results showed average changes in these aerosol species in Beijing of −14.6%, 26.6%, 21.2%, 37.1%, and 38.1% over 21–27 February 2014, which were higher than the results in *J. Wang et al.* [2014], except for SO_4^{2-}. The differences between these two studies might result from the differences in simulated $PM_{2.5}$ concentrations. The simulated $PM_{2.5}$ concentration in Beijing averaged over 12–24 January was 143.7 μg m^{-3} in *J. Wang et al.* [2014], while the concentration averaged over 21–27 February in this work was approximately 348 μg m^{-3}.

BC and OC are chemically inert tracers that respond to changes in meteorological parameters. The percentage changes in OC (BC) were 28.7% (26.7%), 3.2% (3.1%), and 22.3% (22.1%) with the direct radiative effects of total, absorbing, and scattering aerosols, respectively, averaged over the NCP and 21–27 February 2014. The large percentage increases in primary aerosols mainly resulted from the reduced PBL heights by total and scattering aerosols (Figure 8). In the western NCP, PBL heights were reduced by 20–100 m due to absorbing aerosols, leading to increases in BC and OC concentrations. However, BC and OC concentrations were reduced by 0.5–5 μg $m^{-3}$and 2–10 μg m^{-3} in the eastern NCP due to absorbing aerosols (Figure 11), which can be attributed to the changes in atmospheric circulation in this area. As shown in Figure 8, absorbing aerosols induced anomalous northeasterlies that brought relatively clean air from northeastern China to the eastern NCP. The reductions in the concentrations of BC and OC in eastern NCP reflect the dominant role of changes in atmospheric circulation.

For secondary aerosols (SO_4^{2-}, NO_3^-, and NH_4^+), the changes in the concentrations due to the direct radiative effects of aerosols depended on the changes in meteorological variables and on changes in the concentrations of aerosol precursors. Averaged over 21–27 February 2014, and over the NCP, percent changes in SO_4^{2-} were smaller than those of primary aerosols (BC and OC) with values of 11.5%, −1.9%, and 13.5% with total, absorbing, and scattering aerosols, respectively. In addition to the impacts on the concentrations of SO_4^{2-} by changes in PBL height and atmospheric circulation, SO_4^{2-} formation was also influenced by the concentrations of oxidants (such as, OH radicals, O_3, and H_2O_2), crustal aerosols (consisting of catalytic ions, such as, Fe and Mn), and chemical reaction rates. High concentrations of OH radicals, SO_4^{2-} oxidants, and crustal aerosols favored the formation of SO_4^{2-}. Furthermore, high temperatures increased the chemical reaction rates of sulfate formation. Figure 12 shows the spatial distributions of percentage changes in concentrations of OH radicals, H_2O_2, O_3, HNO_3, and crustal aerosols due to the direct radiative effects of aerosols. The direct radiative effects of aerosols reduced solar radiation and the photolysis rates, leading to the inhibited formation of OH radicals, O_3, and H_2O_2. Considering the radiative effects of scattering aerosols, the maximum increase of SO_4^{2-} in Beijing and Tianjin was 20–40% (Figure S2), which were the combined effects of enhanced atmospheric accumulation due to reduced PBL height (Figure 8) and reduced concentrations of OH radicals and sulfate oxidants (O_3, H_2O_2). In contrast, SO_4^{2-} concentrations in the northeastern NCP reduced by 2–15 μg m^{-3} caused by the direct radiative effect of absorbing aerosols. The crustal aerosol concentrations reduced by 5–30% in Tianjin and eastern Beijing due to changes in horizontal wind (Figure 8), which suppressed the aqueous formation of SO_4^{2-}. Furthermore, reductions in the concentrations of the OH radical, O_3, and H_2O_2 contributed to the decreases in SO_4^{2-} in this area.

Averaged over the NCP and 21–27 February 2014, concentrations of NO_3^- increased by 29.5%, 1.3%, and 23.4% caused by the direct radiative effects of total, absorbing, and scattering aerosols, respectively. These percentage increases due to total and scattering aerosols were slightly higher than the simultaneous increases in primary aerosols. While the changes in PBL height had the effect of increasing concentrations of NO_3^-, the reductions in temperature by radiative effects of total and scattering aerosols (Figure 8) favored the formation of NO_3^- [*H. Liao et al.*, 2006]. In Figure S2, the percentage reductions in NO_3^- concentrations due to BC absorption (5–40%) were higher than those of primary aerosols (5–30%) in Tianjin and east of Beijing, which can be attributed to the decreases in HNO_3 concentrations in these locations (Figure 12).

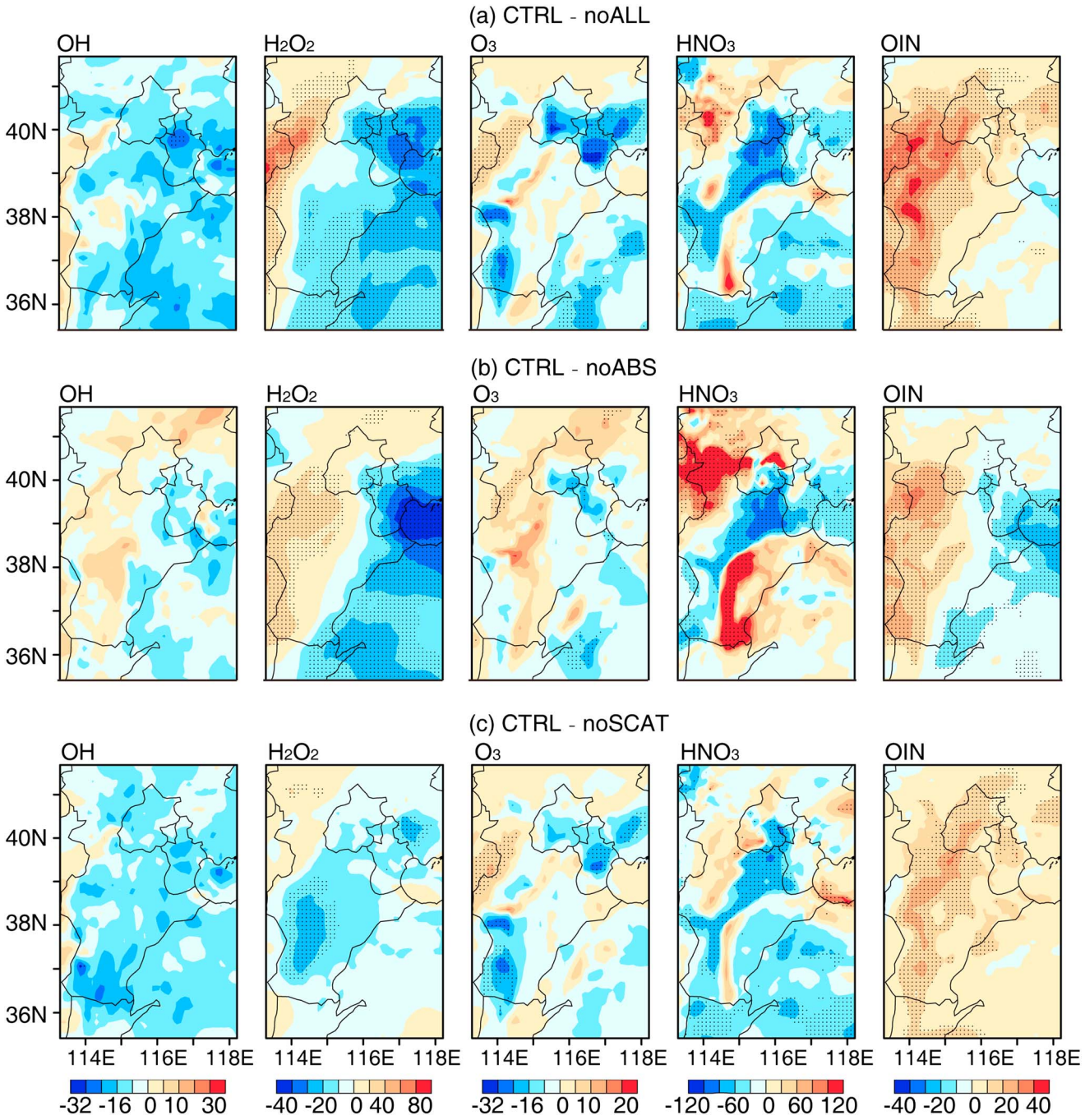

Figure 12. Spatial distributions of the percentage changes (%) of the surface layer concentrations of OH, H_2O_2, O_3, HNO_3, and crustal aerosols (OIN) due to the direct radiative effects of (a) total, (b) absorbing, and (c) scattering aerosols averaged during 21–27 February 2014. The dotted areas are statistically significant at the 95% level, as determined by a two-sample Student's *t* test.

NH_4^+ concentrations were increased by 29.6%, 4.1%, and 22.7% owing to the direct radiative effects of total, absorbing, and scattering aerosols, respectively, averaged over 21–27 February and over the NCP. The spatial patterns of changes in NH_4^+ were similar to those of NO_3^-. The percentage increases due to total and scattering aerosols were slightly larger than the simultaneous increases in primary aerosols, which can also be explained by the enhanced formation of ammonium nitrate.

Table 2 shows the mean changes in $PM_{2.5}$ concentrations due to total, absorbing and scattering aerosols during severe haze days in the NCP. The samples were simulated daily $PM_{2.5}$ concentrations over the NCP region

Table 2. Mean Changes in $PM_{2.5}$ Concentrations ($\mu g\ m^{-3}$) Due To Total, Absorbing and Scattering Aerosols During Severe Haze Days in the NCP[a]

	Daily $PM_{2.5}$ Concentrations ($\mu g\ m^{-3}$)					
	150–250	250–350	350–450	450–550	550–650	650–750
Absorbing aerosols ($\mu g\ m^{-3}$)	−13.2 (−6.4%)	−2.7 (−0.9%)	26.1 (6.7%)	94.9 (19.2%)	126.7 (21.6%)	166.8 (24.0%)
Scattering aerosols ($\mu g\ m^{-3}$)	20.7 (10.1%)	38.0 (12.8%)	77.7 (19.9%)	167.3 (33.8%)	198.9 (33.9%)	269.8 (38.8%)
Total aerosols ($\mu g\ m^{-3}$)	16.1 (7.8%)	45.6 (15.4%)	101.8 (26.1%)	209.2 (42.3%)	269.7 (45.9%)	378.4 (54.4%)
Absorbing aerosols with 50% BC emissions ($\mu g\ m^{-3}$)	−7.0 (−3.4%)	−4.4 (−1.5%)	16.0 (4.1%)	44.3 (8.9%)	78.4 (13.3%)	111.2 (16.3%)
Number of samples (Percentage of samples)	6470 (45.2%)	5234 (36.6%)	1907 (13.3%)	470 (3.3%)	153 (1.1%)	72 (0.5%)

[a]Severe haze days are defined as days with daily $PM_{2.5}$ concentrations larger than 150 $\mu g\ m^{-3}$, following *Cai et al.* [2017]. The samples are daily $PM_{2.5}$ concentrations over the NCP region during 21–27 February and are divided into six groups based on $PM_{2.5}$ concentrations in the CTRL case. The changes in $PM_{2.5}$ concentrations due to BC radiative effects with 50% BC emissions are also represented. The percentage changes are denoted in the brackets. Number of samples in each group and the corresponding proportion of samples in each group to those in six groups are also presented.

during the haze event, which were divided into six groups based on $PM_{2.5}$ concentrations in the CTRL simulation. The percentage changes in the $PM_{2.5}$ concentration due to the feedback were larger when the surface layer $PM_{2.5}$ concentrations were higher. The feedbacks were nonlinear; the percentage change in $PM_{2.5}$ concentrations with total aerosols was not equal to the sum of the change with scattering aerosols and that with absorbing aerosols. Absorbing aerosols induced reductions in $PM_{2.5}$ concentrations with simulated $PM_{2.5}$ concentrations in the CTRL simulation less than 350 $\mu g\ m^{-3}$, which can be explained by the leading role of changes in horizontal wind.

5. Uncertainties in Model Results

The results presented in the previous sections indicated that the radiative feedbacks of aerosols have large impacts on meteorological variables and the surface layer concentrations of chemical species over the NCP during the severe haze event. These results relied on model performance in simulating the concentrations and optical properties of $PM_{2.5}$ and its components. As shown in Figure 3, the BC concentration in Beijing was overestimated by about onefold by the WRF-Chem model. We therefore performed CTRL_0.5BC and noABS_0.5BC simulations to examine the sensitivity of our model results to the simulated BC concentrations. BC emissions were reduced by 50% over the three nested model domains in these two cases, compared with the CTRL simulation.

With BC emissions reduced by 50%, the reductions in PBL height and shortwave flux at the surface by direct radiative effect of absorbing aerosols (CTRL_0.5BC-noABS_0.5BC) were 17.8 m and 9.8 W m^{-2}, respectively, averaged over NCP and 21–27 February. These were approximately one half of the impacts of absorbing aerosol with standard BC emissions (CTRL-noABS). The daily percentage changes in $PM_{2.5}$ concentrations due to absorbing aerosols with 50% BC emissions during severe haze days in the NCP were 4.1%, 8.9%, and 13.3% (Table 2) when the surface $PM_{2.5}$ concentrations were in the range of 350–450 $\mu g\ m^{-3}$, 450–550 $\mu g\ m^{-3}$, and 550–650 $\mu g\ m^{-3}$, which were smaller than those for the base case (6.7%, 19.2%, and 21.6%). These results suggest that the contributions of BC absorption to aerosol feedbacks were important, although BC accounted for only a small fraction of the $PM_{2.5}$ mass concentration.

In our study, SO_4^{2-} concentrations were underestimated and NO_3^- concentrations were overestimated (section 3.2). Although the model captured well the total concentration of scattering aerosols, the responses of sulfate and nitrate to aerosol direct radiative effects might be affected through the uncertainties in aerosol formation. Previous studies pointed out that the production rate of SO_4^{2-} was high under high relative humidity in the NCP in winter [*Zheng et al*., 2015; *Gao et al*., 2016b; *Wang et al*., 2016]. The overestimation of NO_3^- concentration could exaggerate the absolute changes in nitrate concentration due to aerosol radiative effects. The SOA formation over the NCP in winter was not included in this study, which was also important for haze in China [*R. J. Huang et al*., 2014].

Uncertainties associated with our model results also arose from the model performance in simulating PBL height and atmospheric circulation. As shown in section 4, PBL height was underestimated in our study, which partly explained the overestimation of $PM_{2.5}$ concentrations (Figure 2) and led to larger changes in surface layer $PM_{2.5}$ concentrations by aerosol radiative feedbacks. Furthermore, WS10 was overestimated by

58.6% in the NCP during 21–27 February 2014, which also contributed to the simulated aerosol radiative feedbacks on the surface layer concentrations of air pollutants.

6. Conclusions

In this study, we examined the feedbacks of aerosol direct radiative effects onto $PM_{2.5}$ and its components in the NCP during a severe haze event in 21–27 February 2014, using the online-coupled regional chemistry-climate model, WRF-Chem. Sensitivity studies were carried out to quantify the roles of the radiative effects of scattering and absorbing aerosols separately and together.

During the severe haze event in 21–27 February 2014, the observed $PM_{2.5}$ concentrations had a mean value of 202.7 $\mu g\ m^{-3}$ over NCP and highest values of 300–400 $\mu g\ m^{-3}$ in the western Hebei Province. Observations showed high T2 and RH2 values, whereas low WS10 during 21–26 February, favoring the formation of the haze event. Model evaluation showed that the WRF-Chem model reproduced the temporal variation of surface layer meteorological parameters well in the NCP with *R*s of 0.96, 0.82, and 0.84 for T2, RH2, and WS10, respectively. However, it overestimated WS10 by 58.6%. Comparisons of simulated and observed aerosol concentrations in the NCP during 21–27 February showed that the WRF-Chem model captured the spatial and temporal variations of $PM_{2.5}$ concentrations over the NCP during 21–27 February with a *R* of 0.85, but overestimated the concentrations by 21.7%. For aerosol components, the model underestimated concentrations of SO_4^{2-} by about 66% and overestimated BC concentrations by approximately onefold in Beijing during 24–27 February.

In the simulation results averaged over NCP and 21–27 February 2014, the direct radiative effects of total, absorbing, and scattering aerosols reduced the shortwave radiation fluxes at the surface by 54.6 $W\ m^{-2}$, 18.0 $W\ m^{-2}$, and 36.1 $W\ m^{-2}$, respectively. The T2 values were reduced by 1.7°C, 0.2°C, and 1.6°C, and the PBL heights were reduced by 111.4 m, 35.7 m, and 70.7 m, respectively. The changes in meteorological variables induced by scattering aerosols were greater than those due to absorbing aerosols. While scattering aerosols had a small impact on wind in the NCP, absorbing aerosols induced strong anomalous northeasterlies in the eastern NCP.

The direct radiative effects of aerosols caused feedbacks onto the concentrations of chemical species through the above changes in meteorological parameters. With the direct radiative effects of total aerosols, aerosol concentrations over the NCP during 21–27 February 2014 showed average increases of 11.5% for SO_4^{2-}, 29.5% for NO_3^-, 29.6% for NH_4^+, 28.7% for BC, 26.7% for OC, and 20.4% for $PM_{2.5}$, respectively. The increases in primary aerosols (BC and OC) were mainly caused by the changes in PBL height and atmospheric circulation. The changes in secondary aerosols were also related to changes in chemical reaction rates and the concentrations of precursors and oxidants. For example, the maximum increase of SO_4^{2-} in Beijing and Tianjin was 20–40%, as a result of the combined effects of enhanced atmospheric accumulation due to reduced PBL height and reduced concentrations of OH, O_3, and H_2O_2. The changes in the concentrations of SO_4^{2-}, NO_3^-, NH_4^+, OC, BC, and $PM_{2.5}$ due to the direct radiative effects of absorbing aerosols, averaged over the NCP and 21–27 February, were $-0.2\ \mu g\ m^{-3}$ (−1.9%), $0.8\ \mu g\ m^{-3}$ (1.3%), $0.7\ \mu g\ m^{-3}$ (4.1%), $0.7\ \mu g\ m^{-3}$ (3.2%), $0.3\ \mu g\ m^{-3}$ (3.1%), and $2.1\ \mu g\ m^{-3}$ (1.0%), respectively. These are much lower than the increases induced by the direct radiative effects of scattering aerosols. The decreases in $PM_{2.5}$ concentrations in eastern NCP were attributed to the anomalous northeasterlies that transport relatively clean air from northeastern China to the eastern NCP.

By sampling the simulated daily $PM_{2.5}$ concentrations over the NCP during 21–27 February 2014, the model results showed that the percentage increases in $PM_{2.5}$ concentration due to the feedback were greater as the surface layer $PM_{2.5}$ concentrations were higher. The feedback effects of absorbing aerosols were found to either decrease or increase $PM_{2.5}$ concentrations depending on the leading role of BC-induced changes in horizontal wind and PBL heights.

Acknowledgments

This work was supported by the National Basic Research Program of China (973 program, grant 2014CB441202), and the National Natural Science Foundation of China (grants 91544219, 41475137, and 41321064). We acknowledge the NOAA National Climatic Data Center meteorology data set (https://gis.ncdc.noaa.gov/maps/ncei/cdo/hourly), radiosonde data provided by the University of Wyoming (http://weather.uwyo.edu/upperair/sounding.html), anthropogenic emissions from HTAP (http://edgar.jrc.ec.europa.eu/htap_v2/index.php?SECURE=123), concentrations of $PM_{2.5}$, NO_2, SO_2, and O_3 from CNEMC (http://106.37.208.233:20035/), the concentrations of speciated aerosols (SO_4^{2-}, NO_3^-, NH_4^+, BC, and OC) in Jinan provided by Bing Chen [*Chen et al.*, 2016], and AERONET Level 1.5 data sets (https://aeronet.gsfc.nasa.gov/). We also thank Li Liao for his help in developing the emission processing code. The observed concentrations of speciated aerosols in Beijing and WRF-Chem model results have been archived by the corresponding author, Hong Liao (hongliao@nuist.edu.cn) and are available at http://159.226.119.84/~qyl/.

References

Aw, J., and M. J. Kleeman (2003), Evaluating the first-order effect of intraannual temperature variability on urban air pollution, *J. Geophys. Res.*, *108*(4365), 4365, doi:10.1029/2002JD002688.

Barnard, J. C., J. D. Fast, G. Paredes-Miranda, W. P. Arnott, and A. Laskin (2010), Technical note: Evaluation of the WRF-Chem "Aerosol Chemical to Aerosol Optical Properties" module using data from the MILAGRO campaign, *Atmos. Chem. Phys.*, *10*, 7325–7340, doi:10.5194/acp-10-7325-2010.

Bellouin, N., J. Rae, A. Jones, C. Johnson, J. Haywood, and O. Boucher (2011), Aerosol forcing in the Climate Model Intercomparison Project (CMIP5) simulations by HadGEM2-ES and the role of ammonium nitrate, *J. Geophys. Res.*, *116*, D20206, doi:10.1029/2011JD016074.

Binkowski, F. S., and U. Shankar (1995), The regional particulate matter model: 1. Model description and preliminary results, *J. Geophys. Res.*, *100*, 26,191–26,209, doi:10.1029/95JD02093.

Cai W., K. Li, H. Liao, H. Wang, and L. Wu (2017), Weather conditions conducive to Beijing severe haze more frequent under climate change, *Nat. Clim. Change,* doi:10.1038/nclimate3249.

Chan, C. K., and X. Yao (2008), Air pollution in mega cities in China, *Atmos. Environ.*, *42*, 1–42, doi:10.1016/j.atmosenv.2007.09.003.

Chang, W. Y., and H. Liao (2009), Anthropogenic direct radiative forcing of tropospheric ozone and aerosols from 1850 to 2000 estimated with IPCC AR5 emissions inventories, *Atmos. Oceanic Sci. Lett.*, *2*, 201–207, doi:10.1080/16742834.2009.11446804.

Chapman, E. G., W. I. Gustafson, R. C. Easter, J. C. Barnard, S. J. Ghan, M. S. Pekour, and J. D. Fast (2009), Coupling aerosol-cloud-radiative processes in the WRF-Chem model: Investigating the radiative impact of elevated point sources, *Atmos. Chem. Phys.*, *9*, 945–964, doi:10.5194/acp-9-945-2009.

Che, H. et al. (2014), Column aerosol optical properties and aerosol radiative forcing during a serious haze-fog month over North China Plain in 2013 based on ground-based sunphotometer measurements, *Atmos. Chem. Phys.*, *14*, 2125–2138, doi:10.5194/acp-14-2125-2014.

Chen, B., Z. Bai, X. Cui, J. Chen, A. Andersson, and O. Gustafsson (2016), Light absorption enhancement of black carbon from urban haze in northern China winter, *Environ. Pollut.*, *221*, 418–426, doi:10.1016/j.envpol.2016.12.004.

Chen, L. W. A., J. C. Chow, B. G. Doddridge, R. R. Dickerson, W. F. Ryan, and P. K. Mueller (2003), Analysis of a summertime $PM_{2.5}$ and haze episode in the mid-Atlantic region, *J. Air Waste Manage. Assoc.*, *53*, 946–956, doi:10.1080/10473289.2003.10466240.

Curci, G., et al. (2015), Uncertainties of simulated aerosol optical properties induced by assumptions on aerosol physical and chemical properties: An AQMEII-2 perspective, *Atmos. Environ.*, *115*, 541–552, doi:10.1016/j.atmosenv.2014.09.009.

Dawson, J. P., P. J. Adams, and S. N. Pandis (2007), Sensitivity of $PM_{2.5}$ to climate in the eastern U.S.: A modeling case study, *Atmos. Chem. Phys.*, *7*, 4295–4309, doi:10.5194/acp-7-4295-2007.

Ding, A. J., et al. (2013), Intense atmospheric pollution modifies weather: A case of mixed biomass burning with fossil fuel combustion pollution in eastern China, *Atmos. Chem. Phys.*, *13*, 10545–10554, doi:10.5194/acp-13-10545-2013.

Ding, A. J., et al. (2016), Enhanced haze pollution by black carbon in megacities in China, *Geophys. Res. Lett.*, *43*, 2873–2879, doi:10.1002/2016GL067745.

Emmons, L. K., et al. (2010), Description and evaluation of the model for ozone and related chemical tracers, version 4 (MOZART-4), *Geosci. Model Dev.*, *3*, 43–67, doi:10.5194/gmd-3-43-2010.

Easter, R. C., S. J. Ghan, Y. Zhang, R. D. Saylor, E. G. Chapman, N. S. Laulainen, H. Abdul-Razzak, L. R. Leung, X. Bian, and R. A. Zaveri (2004), MIRAGE: Model description and evaluation of aerosols and trace gases, *J. Geophys. Res.*, *109*, D20210, doi:10.1029/2004JD004571.

Fast, J. D., W. I. Gustafson, R. C. Easter, R. A. Zaveri, J. C. Barnard, E. G. Chapman, G. A. Grell, and S. E. Peckham (2006), Evolution of ozone, particulates, and aerosol direct radiative forcing in the vicinity of Houston using a fully coupled meteorology-chemistry-aerosol model, *J. Geophys. Res.*, *111*, D21305, doi:10.1029/2005JD006721.

Forkel, R., J. Werhahn, A. B. Hansen, S. McKeen, S. Peckham, G. Grell, and P. Suppan (2012), Effect of aerosol-radiation feedback on regional air quality—A case study with WRF/Chem, *Atmos. Environ.*, *53*, 202–211, doi:10.1016/j.atmosenv.2011.10.009.

Gao, M., G. R. Carmichael, Y. Wang, P. E. Saide, M. Yu, J. Xin, Z. Liu, and Z. Wang (2016a), Modeling study of the 2010 regional haze event in the North China Plain, *Atmos. Chem. Phys.*, *16*, 1673–1691, doi:10.5194/acp-16-1673-2016.

Gao, M., G. R. Carmichael, Y. Wang, D. Ji, Z. Liu, and Z. Wang (2016b), Improving simulations of sulfate aerosols during winter haze over northern China: The impacts of heterogeneous oxidation by NO2, *Front. Environ. Sci. Eng.*, *10*(5), 165–175, doi:10.1007/s11783-016-0878-2.

Gao, Y., M. Zhang, Z. Liu, L. Wang, P. Wang, X. Xia, M. Tao, and L. Zhu (2015), Modeling the feedback between aerosol and meteorological variables in the atmospheric boundary layer during a severe fog-haze event over the North China Plain, *Atmos. Chem. Phys.*, *15*, 4279–4295, doi:10.5194/acp-15-4279-2015.

Gao, Y., C. Zhao, X. H. Liu, M. G. Zhang, and L. R. Leung (2014), WRF-Chem simulations of aerosols and anthropogenic aerosol radiative forcing in East Asia, *Atmos. Environ.*, *92*, 250–266, doi:10.1016/j.atmosenv.2014.04.038.

Giorgi F., X. Bi, and Y. Qian (2002), Direct radiative forcing and regional climate effects of anthropogenic aerosols over East Asia: A regional coupled climate-chemistry/aerosol model study, *J. Geophys. Res.*, *107*(107), 4439, doi:10.1029/2001JD001066.

Gong, S. L., L. A. Barrie, and J.-P. Blanchet (1997), Modeling sea-salt aerosols in the atmosphere: 1. Model development, *J. Geophys. Res.*, *102*, 3805–3818, doi:10.1029/96JD02953.

Gong, S. L. (2003), A parameterization of sea-salt aerosol source function for sub- and super-micron particles, *Global Biogeochem. Cycles 17*(D3), 1097, doi:10.1029/2003GB002079.

Grell, G. A., S. E. Peckham, R. Schmitz, S. A. McKeen, G. Frost, W. C. Skamarock, and B. Eder (2005), Fully coupled "online" chemistry within the WRF model, *Atmos. Environ.*, *39*, 6957–6975, doi:10.1016/j.atmosenv.2005.04.027.

Guenther, A., T. Karl, P. Harley, C. Wiedinmyer, P. I. Palmer, and C. Geron (2006), Estimates of global terrestrial isoprene emissions using MEGAN (Model of Emissions of Gases and Aerosols from Nature), *Atmos. Chem. Phys.*, *6*, 3181–3210, doi:10.5194/acp-6-3181-2006.

Holben, B. N., et al. (1998), AERONET—A federated instrument network and data archive for aerosol characterization, *Remote Sens. Environ.*, *66*, 1–16, doi:10.1016/S0034-4257(98)00031-5.

Hong, S. Y., Y. Noh, and J. Dudhia (2006), A new vertical diffusion package with an explicit treatment of entrainment processes, *Mon. Weather Rev.*, *134*, 2318–2341, doi:10.1175/MWR3199.1.

Huang, R. J., et al. (2014), High secondary aerosol contribution to particulate pollution during haze events in China, *Nature*, *514*, 218–222.

Huang, X., Y. Song, C. Zhao, M. Li, T. Zhu, Q. Zhang, and X. Zhang (2014), Pathways of sulfate enhancement by natural and anthropogenic mineral aerosols in China, *J. Geophys. Res. Atmos.*, *119*, 14,165–114,179, doi:10.1002/2014JD022301.

Jiang, F., P. Zhou, Q. Liu, T. Wang, B. Zhuang, and X. Wang (2012), Modeling tropospheric ozone formation over East China in springtime, *J. Atmos. Chem.*, *69*, 303–319, doi:10.1007/s10874-012-9244-3.

Jung, J., H. Lee, Y. J. Kim, X. Liu, Y. Zhang, J. Gu, and S. Fan (2009), Aerosol chemistry and the effect of aerosol water content on visibility impairment and radiative forcing in Guangzhou during the 2006 Pearl River Delta campaign, *J. Environ. Manage.*, *90*, 3231–3244, doi:10.1016/j.jenvman.2009.04.021.

Kleeman, M. J. (2008), A preliminary assessment of the sensitivity of air quality in California to global change, *Clim. Change*, *87*, S273–S292, doi:10.1007/s10584-007-9351-3.

Li, K., H. Liao, Y. Mao, and D. A. Ridley (2015), Source sector and region contributions to concentration and direct radiative forcing of black carbon in China, *Atmos. Environ.*, *124*, 351–366, doi:10.1016/j.atmosenv.2015.06.014.

Li, K., H. Liao, J. Zhu, and J. M. Moch (2016), Implications of RCP emissions on future $PM_{2.5}$ air quality and direct radiative forcing over China, *J. Geophys. Res. Atmos.*, *121*, 12,985–13,008, doi:10.1002/2016JD025623.

Li, M., et al. (2015), MIX: A mosaic Asian anthropogenic emission inventory for the MICS-Asia and the HTAP projects, *Atmos. Chem. Phys. Discuss.*, *15*(23), 34,813–34,869, doi:10.5194/acpd-15-34813-2015.

Liao, H., W. T. Chen, and J. H. Seinfeld (2006), Role of climate change in global predictions of future tropospheric ozone and aerosols, *J. Geophys. Res.*, *111*, D12304, doi:10.1029/2005JD006852.

Liao, L., S. J. Lou, Y. Fu, W. Y. Chang, and H. Liao (2015), Radiative forcing of aerosols and its impact on surface air temperature on the synoptic scale in eastern China [in Chinese], *Chin. J. Atmos. Sci.*, *39*(1), 68–82, doi:10.3878/j.issn.1006-9895.1402.13302.

Liao, L., and H. Liao (2014), Role of the radiative effect of black carbon in simulated $PM_{2.5}$ concentrations during a haze event in China, *Atmos. Oceanic Sci. Lett.*, *7*, 430–440, doi:10.3878/j.issn.1674-2834.14.0023.

Lin, Y. L., R. D. Farley, and H. D. Orville (1983), Bulk parameterization of the snow field in a cloud model, *J. Clim. Appl. Meteorol.*, *22*, 1065–1092, doi:10.1175/1520-0450(1983)022<1065:BPOTSF>2.0.CO;2.

Miao, Y., S. Liu, Y. Zheng, and S. Wang (2016), Modeling the feedback between aerosol and boundary layer processes: A case study in Beijing, China, *Environ. Sci. Pollut. Res. Int.*, *23*, 3342–3357, doi:10.1007/s11356-015-5562-8.

Niu, S. J., C. S. Lu, H. Y. Yu, L. J. Zhao, and J. J. Lu (2010), Fog research in China: An overview, *Adv. Atmos. Sci.*, *27*, 639–662, doi:10.1007/s00376-009-8174-8.

Quan, J., X. Tie, Q. Zhang, Q. Liu, X. Li, Y. Gao, and D. Zhao (2014), Characteristics of heavy aerosol pollution during the 2012–2013 winter in Beijing, China, *Atmos. Environ.*, *88*, 83–89, doi:10.1016/j.atmosenv.2014.01.058.

Racherla, P. N., and P. J. Adams (2006), Sensitivity of global tropospheric ozone and fine particulate matter concentrations to climate change, *J. Geophys. Res.*, *111*, D24103, doi:10.1029/2005JD006939.

Schichtel, B. A., R. B. Husar, S. R. Falke, and W. E. Wilson (2001), Haze trends over the United States, 1980–1995, *Atmos. Environ.*, *35*, 5205–5210, doi:10.1016/S1352-2310(01)00317-X.

Situ, S., A. Guenther, X. Wang, X. Jiang, A. Turnipseed, Z. Wu, J. Bai, and X. Wang (2013), Impacts of seasonal and regional variability in biogenic VOC emissions on surface ozone in the Pearl River delta region, China, *Atmos. Chem. Phys.*, *13*, 11,803–11,817, doi:10.5194/acp-13-11803-2013.

Sun, Y. L., Q. Jiang, Z. F. Wang, P. Q. Fu, J. Li, T. Yang, and Y. Yin (2014), Investigation of the sources and evolution processes of severe haze pollution in Beijing in January 2013, *J. Geophys. Res. Atmos.*, *119*, 4380–4398, doi:10.1002/2014JD021641.

Tie, X., D. Wu, and G. Brasseur (2009), Lung cancer mortality and exposure to atmospheric aerosol particles in Guangzhou, China, *Atmos. Environ.*, *43*, 2375–2377, doi:10.1016/j.atmosenv.2009.01.036.

Wang, G., R. Zhang, M. E. Gomez, L. Yang, M. L. Zamora, M. Hu, Y. Lin, J. Peng, S. Guo, and J. Meng (2016), Persistent sulfate formation from London fog to Chinese haze, *Proc. Natl. Acad. Sci. U.S.A.*, *113*, 13,630–13,635, doi:10.1073/pnas.1616540113.

Wang, H., G. Y. Shi, X. Y. Zhang, S. L. Gong, S. C. Tan, B. Chen, H. Z. Che, and T. Li (2014), Mesoscale modeling study of the interactions between aerosols and PBL meteorology during a haze episode in China Jing-Jin-Ji and its near surrounding region—Part 2: Aerosols' radiative feedback effects, *Atmos. Chem. Phys. Discuss.*, *14*, 28,269–28,298, doi:10.5194/acpd-14-28269-2014.

Wang, J., et al. (2014), Impact of aerosol–meteorology interactions on fine particle pollution during China's severe haze episode in January 2013, *Environ. Res. Lett.*, *9*, 094002, doi:10.1088/1748-9326/9/9/094002.

Wang, T., F. Jiang, J. Deng, Y. Shen, Q. Fu, Q. Wang, Y. Fu, J. Xu, and D. Zhang (2012), Urban air quality and regional haze weather forecast for Yangtze River Delta region, *Atmos. Environ.*, *58*, 70–83, doi:10.1016/j.atmosenv.2012.01.014.

Wang, Y., G. S. Zhuang, Y. L. Sun, and Z. S. An (2006), The variation of characteristics and formation mechanisms of aerosols in dust, haze, and clear days in Beijing, *Atmos. Environ.*, *40*, 6579–6591, doi:10.1016/j.atmosenv.2006.05.066.

Wang, Y. S., L. Yao, L. L. Wang, Z. R. Liu, D. S. Ji, G. Q. Tang, J. K. Zhang, Y. Sun, B. Hu, and J. Y. Xin (2014), Mechanism for the formation of the January 2013 heavy haze pollution episode over central and eastern China, *Sci. China Earth Sci.*, *57*, 14–25, doi:10.1007/s11430-013-4773-4.

Wesely, M. L. (1989), Parameterization of surface resistance to gaseous dry deposition in regional numerical models, *Atmos. Environ.*, *23*, 1293–1304, doi:10.1016/0004-6981(89)90153-4.

Wiedinmyer, C., S. K. Akagi, R. J. Yokelson, and L. K. Emmons (2011), The Fire Inventory from NCAR (FINN): A high resolution global model to estimate the emissions from open burning, *Geosci. Model Dev.*, *4*, 625–641, doi:10.5194/gmd-4-625-2011.

Wild, O., X. Zhu, and M. J. Prather (2000), Fast-J: Accurate simulation of in- and below-cloud photolysis in tropospheric chemical models, *J. Atmos. Chem.*, *37*, 245–282, doi:10.1023/A:1006415919030.

Yadav, A. K., K. Kumar, A. Kasim, M. P. Singh, S. K. Parida, and M. Sharan (2003), Visibility and incidence of respiratory diseases during the 1998 haze episode in Brunei Darussalam, *Pure Appl. Geophys.*, *160*, 265–277, doi:10.1007/s00024-003-8777-4.

Yang, Y., H. Liao, and S. Lou (2016), Increase in winter haze over eastern China in the past decades: Roles of variations in meteorological parameters and anthropogenic emissions, *J. Geophys. Res. Atmos.*, *121*, 13,050–13,065, doi:10.1002/2016JD025136.

Yang, Y. R., et al. (2015), Characteristics and formation mechanism of continuous hazes in China: A case study during the autumn of 2014 in the North China Plain, *Atmos. Chem. Phys.*, *15*, 8165–8178, doi:10.5194/acp-15-8165-2015.

Yu, M., G. R. Carmichael, T. Zhu, and Y. Cheng (2012), Sensitivity of predicted pollutant levels to urbanization in China, *Atmos. Environ.*, *60*, 544–554, doi:10.1016/j.atmosenv.2012.06.075.

Zaveri, R. A., and L. K. Peters (1999), A new lumped structure photochemical mechanism for large-scale applications, *J. Geophys. Res.*, *104*, 30,387–30,415, doi:10.1029/1999JD900876.

Zaveri, R. A., R. C. Easter, J. D. Fast, and L. K. Peters (2008), Model for Simulating Aerosol Interactions and Chemistry (MOSAIC), *J. Geophys. Res.*, *113*, D13204, doi:10.1029/2007JD008782.

Zhang, B., Y. X. Wang, and J. M. Hao (2014), Simulating aerosol–radiation–cloud feedbacks on meteorology and air quality over eastern China under severe haze conditions in winter, *Atmos. Chem. Phys. Discuss.*, *14*, 26,085–26,125, doi:10.5194/acpd-14-26085-2014.

Zhang, Y., W. Huang, T. Cai, D. Fang, Y. Wang, J. Song, M. Hu, and Y. Zhang (2016), Concentrations and chemical compositions of fine particles ($PM_{2.5}$) during haze and non-haze days in Beijing, *Atmos. Res.*, *174-175*, 62–69, doi:10.1016/j.atmosres.2016.02.003.

Zhang, Y., X. Y. Wen, and C. J. Jang (2010), Simulating chemistry-aerosol-cloud-radiation-climate feedbacks over the continental US using the online-coupled Weather Research Forecasting model with chemistry (WRF/Chem), *Atmos. Environ.*, *44*, 3568–3582, doi:10.1016/j.atmosenv.2010.05.056.

Zhao, C., L. R. Leung, R. Easter, J. Hand, and J. Avise (2013), Characterization of speciated aerosol direct radiative forcing over California, *J. Geophys. Res. Atmos.*, *118*, 2372–2388, doi:10.1029/2012JD018364.

Zhao, C., X. Liu, L. R. Leung, B. Johnson, S. A. McFarlane, W. I. Gustafson, J. D. Fast, and R. Easter (2010), The spatial distribution of mineral dust and its shortwave radiative forcing over North Africa: Modeling sensitivities to dust emissions and aerosol size treatments, *Atmos. Chem. Phys.*, *10*, 8821–8838, doi:10.5194/acp-10-8821-2010.

Zhao, C., X. Liu, L. R. Leung, and S. Hagos (2011), Radiative impact of mineral dust on monsoon precipitation variability over West Africa, *Atmos. Chem. Phys.*, *11*, 1879–1893, doi:10.5194/acp-11-1879-2011.

Zhao, X. J., P. S. Zhao, J. Xu, W. Meng, W. W. Pu, F. Dong, D. He, and Q. F. Shi (2013), Analysis of a winter regional haze event and its formation mechanism in the North China Plain, *Atmos. Chem. Phys.*, *13*, 5685–5696, doi:10.5194/acp-13-5685-2013.

Zheng, B., Q. Zhang, Y. Zhang, K. B. He, K. Wang, G. J. Zheng, F. K. Duan, Y. L. Ma, and T. Kimoto (2015), Heterogeneous chemistry: A mechanism missing in current models to explain secondary inorganic aerosol formation during the January 2013 haze episode in north China, *Atmos. Chem. Phys.*, *14*(15), 2031–2049.